Transcriptomic landscapes of SARS-CoV-2-infected and bystander lung cells reveal a selective upregulation of NF-κB-dependent coding and non-coding proviral transcripts

Ugo Szachnowski[1#], Anvita Bhargava[2#], Maxime Chazal[2#], Dominika Foretek[1,2], Sophie-Marie Aicher[2], Juliana Pipoli da Fonseca[3], Patricia Jeannin[4], Guillaume Beauclair[5], Marc Monot[3], Antonin Morillon[1]*, Nolwenn Jouvenet[2]*

# These authors contributed equally to this work.
* co-corresponding authors

[1] *CNRS UMR3244, Sorbonne University, PSL University, Institut Curie, Centre de Recherche, Paris, France*
[2] *Institut Pasteur, Université de Paris, CNRS UMR 3569, Virus sensing and signaling Unit, Paris, France*
[3] *Institut Pasteur, Université de Paris, Biomics Platform, C2RT, Paris, France*
[4] *Institut Pasteur, Université de Paris, CNRS UMR 3569, Unité Épidémiologie et Physiopathologie des Virus Oncogènes, Paris, France*
[5] *Université Paris-Saclay, CEA, CNRS, Institute for Integrative Biology of the Cell (I2BC), Gif-sur-Yvette, France*

Abstract

Detailed knowledge of cellular networks that are modulated by Severe acute respiratory syndrome coronavirus 2 (SARS-CoV-2) is needed to understand viral replication and host response. So far, transcriptomic analyses of interactions between SARS-CoV-2 and cells were performed on mixed populations of infected and uninfected cells or using single-cell RNA sequencing, both leading to inaccurate or low-resolution gene expression interpretations. Moreover, they generally focused on annotated messenger RNAs (mRNAs), ignoring other transcripts, such as long non-coding RNAs (lncRNAs) and unannotated RNAs. Here, we performed deep polyA$^+$ transcriptome analyses of lung epithelial A549 cells infected with SARS-CoV-2, which were sorted based on the expression of the viral protein spike (S). To increase the sequencing depth and improve the robustness of the analysis, the samples were depleted of viral transcripts. Infection caused a massive reduction in mRNAs and lncRNAs, including transcripts coding for antiviral innate immune proteins, such as interferons (IFNs). This absence of IFN response probably explains the poor transcriptomic response of bystander cells co-cultured with spike positive (S$^+$) ones. NF-κB and inflammatory response were among the pathways that escaped the global shutoff in S$^+$ cells. In agreement with the RNA-seq analysis, inflammatory cytokines, but not IFNs, were produced and secreted by infected cells. Functional investigations revealed the proviral function of the NF-kB subunit p105/p50 and some of its known target genes, including IL32 and IL8, as well as the lncRNA ADIRF-AS1, which we identified as a novel NF-kB target gene. Thus, analyzing the polyA$^+$ transcriptome of sorted populations of infected lung cells allowed unprecedented identification of cellular functions that are directly affected by infection and the recovery of coding and non-coding genes that contribute to SARS-CoV-2 replication.

Introduction

Severe acute respiratory syndrome coronavirus 2 (SARS-CoV-2) is the causative agent of Coronavirus Disease-2019 (COVID-19). The virus emerged in Wuhan, China, at the end of 2019 and has since spread around the globe. SARS-CoV-2 infection may be asymptomatic or it may cause a wide spectrum of symptoms, from mild upper respiratory tract infection to life-threatening pneumonia [1]. Viral replication is not limited to the respiratory tract, but rather occurs in numerous organs, including the blood, heart, vessels, intestines, brain and kidneys [2]. The mortality rate of SARS-CoV-2 infection is estimated at 3%–4%, compared with a mortality rate of less than 1% from influenza [3]. Severity of the disease correlates with an excessive pro-inflammatory immune response [4–6], which may be responsible for the symptoms observed in patients. Inflammation is a vital defense mechanism that is required to initiate an adaptive immune response *via* the recruitment and activation of immune cells. However, the non-resolution of acute inflammation leads to tissue damage [7].

SARS-CoV-2 infection is also characterized by a suppression of interferon (IFN) response in infected cells [8]. IFNs are potent antiviral cytokines secreted by various cell types. In virus-infected cells, the IFN response is initiated by the recognition of viral nucleic acids by cellular receptors. Once

activated, these receptors recruit adaptor proteins and kinases that trigger the nuclear translocation of the transcription factors IRF3 and NF-κB, which, in turn, induce the rapid expression of IFNs and proinflammatory cytokines [9]. In particular, type I (IFNα and β) and type III (IFN-λ1 and IFN-λ2/3) IFNs play crucial roles in protecting infected and neighboring cells from virus replication and spread. Once secreted, they will signal in a paracrine and autocrine manner through their receptors, resulting in the activation of the transcription factor complex ISGF3, which subsequently induces the expression of up to approximately 2000 IFN-stimulated genes (ISGs). Many of these ISGs block the viral life cycle by targeting specific stages of replication, including entry into host cells, protein translation, replication or assembly of new virus particles. Some ISGs are specific to a virus or a viral family, while others are broad-spectrum. Their concerted actions establish the antiviral state [10,11]. Like all viruses [12], SARS-CoV-2 overcomes IFN responses *via* a wide array of mechanisms involving viral proteins [13–15] and a virus-derived microRNA [16,17]. These viral strategies likely contribute to an impaired IFN response in COVID-19 patients [18] and, consequently, high levels of viral replication.

A large effort has been undertaken to understand the molecular mechanism underlying the lack of IFN response and the overproduction of inflammatory cytokines in SARS-CoV-2 infected cells. Numerous transcriptomic analyses of human cells infected with SARS-CoV-2 have been performed to describe the perturbation of cellular pathways induced by infection, using several cellular models, such as human cells derived from lung, bronchial or colorectal tissue [19–21], as well as post-mortem lung samples of COVID-19 patients [19] and bronchoalveolar lavage fluids (BALF) from patients [22]. These genome-wide investigations of host cellular responses to SARS-CoV-2 infection were performed exclusively using bulk RNA-sequencing (RNA-seq) technologies, *i.e.* by analyzing gene perturbations in mixed populations of infected and uninfected cells. Previous studies on Zika virus infected cells have estimated that only 10% of the repressed and about 30% of the induced genes can be identified in a mixed population containing around one third of infected cells [23]. Bulk transcriptome signals are thus partly drawn into noise background, rendering impossible to efficiently and exhaustively portray the full variation of the host transcripts.

The perturbation of cellular responses in SARS-CoV-2 infected and bystander cells have also been analyzed using single-cell (sc) RNA-seq methods. Such studies were performed in a variety of cellular models, including COVID-relevant ones, such as human intestinal organoids [24], human tracheal-bronchial epithelial cells [25,26], human lung cell lines [21] and BALF from patients [27]. However, the technical variability, high noise and massive sample size of scRNA-seq data raise challenges in analyzing the total number of differentially expressed genes (DEGs) [28] out of a limited list of only 1000 to 3000 most expressed genes in individual cells. The balance between the number of cells to be sequenced and the sequencing depth to extract the maximum amount of information from the experiment also affects the results [29].

Moreover, most bulk and single-cell transcriptomic studies performed to investigate the cellular response to SARS-CoV-2 focused on the expression of the referenced coding genome, largely ignoring

non-coding and unannotated information, mainly represented by long non-coding RNAs (lncRNAs). These RNAs, which are at least 200 nucleotides (nt) in length, are of specific interest since they play fundamental roles in cellular identity, development and disease progression through epigenetic or post-transcriptional regulation of mRNA expression [30]. Combined RNA-seq data from multiple sources reported over 58000 lncRNA loci in the human genome [31]. Future studies will plausibly increase this number, since lncRNAs are more cell-type specific [32] and expressed at lower levels than mRNAs [31]. Most of them are independently transcribed by RNA polymerase II and, like protein-coding RNAs, they can be 5'-capped, polyadenylated, and spliced by the cellular machinery [33]. Increasing evidence suggests the involvement of lncRNAs in virus-host interactions and antiviral immunity [34,35]. Current efforts are under progress to uncover, in different contexts, the unannotated RNAs that could encompass a variety of RNA biotypes, from rare mRNA isoforms to unannotated intergenic long noncoding RNAs, using reference-based approach with the human gencode annotation [36] or unreferenced-based methods for unmappable transcripts [37]. However, so far, none of these strategies have been engaged to dissect virus-cell interactions.

Here, we investigated the coding and non-coding transcriptional landscape of lung cells infected with SARS-CoV-2 and sorted according to the expression of the viral protein spike (S). Our deep transcriptome analysis using annotated RNA genes and reference-based RNA profiler uncovered pathways that are directly affected by infection and identified coding and non-coding genes contributing to an optimal SARS-CoV-2 replication.

Results

Transcriptional landscapes of SARS-CoV-2 infected and bystander lung cells uncovers a global expression shutoff

To analyze transcriptomic changes in infected and bystander cells, human alveolar basal epithelial carcinoma cells (A549) stably expressing the viral receptor ACE2 (A549-ACE2) were infected with a MOI of 1 for 24 hours, fixed, stained intracellularly using antibodies against S proteins and sorted into S-positive (infected cells, S^+) and S-negative (bystander, S^-) populations (Fig. 1A and 1B). Around 15% of A549-ACE2 cells were positive for S protein (Fig. 1B). Cells negative for S protein represent either uninfected cells or cells at an early stage of infection, prior to viral protein production. Mock-infected cells served as negative controls. The experiment was performed twice independently in triplicates. PolyA+ RNAs were isolated from mock-infected, S^+ and S^- cells. Around 85% of the total reads mapped to the viral genome in S^+ cells, while less than 5% of the total reads aligned with the viral genome in S^- cells (Fig. 1C), validating our sorting approach. The large dominance of viral reads over cellular reads illustrates the ability of the virus to hijack the cellular machinery for its replication. A similar proportion of SARS-CoV-2 reads in the RNA pool was previously reported in lung epithelial carcinoma Calu-3 cells infected for 8 hours [20]. These differences in the representation of viral RNA between S^+ and S^-

139 cells altered the robustness of the statistical analysis used to identify DEGs. To overcome this limitation,
140 the samples were depleted of viral RNAs (vRNAs) using a set of oligonucleotide probes covering the
141 entire viral genome (Fig. 1A). Following depletion, viral reads represented between 0,01 and 2,8% of
142 the total reads both in S^+ and S^- cells (Fig. 1C).

143 Coding and long non-coding genes were identified using gencode annotation (v32), while
144 unannotated RNAs were recovered with Scallop assembler [36] (Fig. 1D-F, Fig. S1 and tables S1-S3).
145 Principal component analysis (PCA) of polyA+ transcriptomes segregated S^+ cells from S^- and mock-
146 infected ones (Fig. 1D). This segregation based on S expression represented around 92% of the
147 transcriptomic differences between the samples (Fig. 1D). Only subtle differences (2,5%) distinguished
148 bystander and mock-infected cells (Fig. 1D), suggesting that the transcriptional landscapes of these 2
149 cell populations were very similar. An absence of response of S^- cells was unexpected since cytokines,
150 which are commonly secreted by virally infected cells, activate an antiviral state in bystander cells
151 through surface receptors.

152 Analysis of gene expression allowed identification of thousands of annotated coding and non-
153 coding genes that were differentially expressed (absolute fold change ≥ 2, p-value < 0.05) in S^+ cells as
154 compared to S^- or mock-infected ones (Fig. 1E-F and tables S1-S3). We identified around 13 times more
155 downregulated coding genes than upregulated ones in S^+ cells (Fig. 1E-F), suggesting that infection
156 triggers a massive, but incomplete, shutoff of gene expression. Among the top upregulated coding genes
157 in S^+ cells, we confirmed candidates revealed by previous analyses performed in non-sorted non-vRNA-
158 depleted A549-ACE2 cells, such as CXCL8, CCL20, IL6 and NFKB1 [19,38,39], but also novel highly
159 significant candidates, including IL32 and ITGAM (table S1). The genes encoding IFN type I and type
160 III were not significantly upregulated in S^+ cells, as compared to mock-infected cells. Accordingly, ISGs
161 were not upregulated either in S^+ cells. This absence of innate immune response in infected cells agrees
162 with previous analyses performed in mixed population of A549-ACE2 cells infected with SARS-CoV-
163 2 [19,38,39]. Such absence of innate response reflects the ability of the virus to potently inhibit the IFN
164 response *via* numerous mechanisms in human cells [14]. Around 1260 annotated lncRNAs were
165 downregulated in S^+ cells as compared to mock-infected cells, and 184 were upregulated (Fig. 1E-F and
166 table S2). RFPL3S, ADIRF-AS1 and WAKMAR2 were among the top 15 upregulated lncRNAs in S^+
167 cells. RFPL3S and ADIRF-AS1 have no known functions, whereas WAKMAR2 restricts NF-kB-
168 induced production of inflammatory chemokines in human keratinocytes [40]. Among the top
169 downregulated lncRNAs, we identified HOXA-AS2 and NKILA, which are negative regulators of NF-
170 kB signaling, in endothelial cells and breast cancer cell lines, respectively [41,42]. Altered expression
171 of WAKMAR2, HOXA-AS2 and NKILA in infected cells could thus play a role in viral-associated
172 inflammation. From the 1400 unannotated transcripts we detected using Scallop assembler [36], around
173 800 unannotated polyA+ transcripts were also differentially expressed in S+ cells as compared to S^-
174 ones (Fig. 1E-F and table S3).

175 In agreement with the PCA (Fig. 1D), volcano plots and heat maps revealed that S^- bystander cells
176 and mock-infected control cells exhibited very similar transcriptomic profiles (Fig. 1E-1F and Fig. S1A-
177 S1B). Only around 170 polyA+ transcripts were differentially expressed in S^- cells as compared to
178 mock-infected ones (Fig. 1E and tables S1-S3). As a comparison, over 13000 DEGs were identified in
179 S^+ as compared to mock-infected cells (Fig. 1E and tables S1-S3). These analyses further suggest that
180 S+ cells present none or very little paracrine signaling response. Among the 69 coding genes that were
181 upregulated in S^- cells as compared to mock-infected, 29 were also upregulated in S^+ cells (Fig. S1B
182 and table S3). Some of these common genes were inflammatory genes, such as IL32, IL6 and CCL20.
183 Among the 39 upregulated coding genes that were unique to S^- cells, 16 were ISGs (examples include
184 MX1, APOL1 and IFI6). The expression of these inflammatory genes and ISGs in bystander cells could
185 be induced early in infection, prior to the production of S proteins.
186 Our approach reveals that SARS-CoV-2 infection triggers a major shutoff of gene expression in
187 A549-ACE2 cells. It also shows that S^- cells do not exhibit a strong transcriptional signature despite
188 being cultured with S^+ cells, suggesting the absence of an efficient paracrine communication.
189
190 **Separating lung cells based on the expression of the viral S protein improved discovery of DEGs**
191 To compare our differential deep analyses with known datasets, we analyze publicly available
192 polyA+ RNA-seq raw data of unsorted A549-ACE2 infected with SARS-CoV-2 at a MOI of 0.2 [19].
193 Viral reads represented around 50% of the total number of reads in these unsorted bulk population of
194 cells [19], which was expectedly less than in A549-ACE2 cells positive for S (Fig. 1C). The 2 analyses
195 shared 150 upregulated protein-coding genes and 238 downregulated ones (Fig. 2A, table S4). The vast
196 majority (about 80%) of the downregulated mRNAs that we identified were classified as 'unchanged'
197 in the analysis of unsorted cells (Fig. 2A, table S4). Thus, sorting cells based on S expression and
198 depleting viral RNA allowed the identification of over 30 times more downregulated coding genes than
199 in unsorted cells (Fig. 2A, table S4). The poor sensibility of analysis of mixed cell population in
200 detecting downregulated genes is likely due to the large proportion of non-infected cells, in which the
201 majority of genes remained normally expressed, thus masking any decrease of gene expression in the
202 pool of infected cells. Indeed, an artificial reconstruction of a mixed cell population (80% S^- and 20%
203 S^+) supports this hypothesis (Fig. S1C). About 41% of the upregulated protein-coding genes and 16%
204 of downregulated ones that we identified did not appear in conventional RNA-seq analysis of mixed
205 populations [19]. This comparison highlights the accuracy and the depth of our analysis.
206 To validate the sorting approach combined with vRNA-depletion, we compared mRNA
207 abundances of a few DEGs in a bulk population of cells infected with SARS-CoV-2 for 24 hours, as
208 well as in sorted S^+ and bystander S^- cells infected in the same condition. As expected, S+ cells produced
209 approximately 200-fold more intracellular viral RNAs than did S^- cells (Fig. 2B). These qPCR analyses
210 confirm that some S^- cells are at an early stage of viral replication, prior to viral protein expression (Fig.
211 1B). We included in the analysis three coding transcripts (IL32, ITGAM and TRAF1), two lncRNAs

212 (WAKMAR2 and AL132990.1) and one unannotated transcript (XLOC_007519) that were identified
213 amongst the most upregulated RNAs in S^+ A549-ACE2 cells (Fig. 2C, S2A and tables S1-S3). The
214 abundance of IL32 mRNA did not increase significantly in the infected bulk population, as compared
215 to mock-infected cells (Fig. 2C). By contrast, IL32 mRNA levels increased around 30-fold in S^+ cells,
216 compared to those in mock-infected cells (Fig. 2C). This difference explains why IL32 was not identified
217 as an up-regulated gene in previous RNA-seq analysis performed in mixed population of infected A549-
218 ACE2 cells [19,38]. Similarly, the expression of ITGAM, TRAF1, WAKMAR2, AL132990.1 and
219 XLOC_007519 showed a modest increase of mRNA abundances in the bulk population and a significant
220 increase in S^+ cells, as compared to mock-infected cells (Fig. 2C and S2B). The decreased expression
221 of transcripts identified as top downregulated hits in the RNA-seq analysis of S+ cells, such as the coding
222 transcripts FEN1 and SNRPF, the lncRNAs AC016747.1, DANCR and TP53TG1, as well as the
223 unannotated RNA XLOC_049236 (Fig. S2A), was significantly more pronounced in S^+ cells than in the
224 mixed population of cells, when compared to mock-infected cells (Fig. 2D and S2C). Analysis of RNA
225 abundances in sorted cells thus highlighted the increased accuracy of our approach, compared to
226 classical methods, in detecting up- and down- regulated genes.
227 To identify pathways affected by infection in A549-ACE2 cells, we performed Gene Ontology
228 (GO) terms and KEGG pathway enrichment analysis on the upregulated coding genes in S^+ cells, as
229 compared to mock-infected cells (Fig. 2E). We observed a significant enrichment in several
230 inflammatory signaling pathways, including TNF and NF-κB signatures, which were previously
231 identified in bulk transcriptomic analysis of infected A549 and Calu-3 cells [38,39] and in scRNA-seq
232 analysis of infected colon and ileum organoids [24]. Members of the superfamily of TNF proteins are
233 multifunctional proinflammatory cytokines. NF-κB plays an important role in promoting inflammation,
234 as well as regulating cell proliferation and survival [43]. Activation of NF-κB is one of the signals
235 transduced by the TNF-superfamily members [44]. These inflammatory signatures are also consistent
236 with those observed in peripheral blood immune cells of severe or critical COVID-19 patients [18].
237
238 **Inflammatory cytokines, but not IFNs, are produced and secreted by infected cells**
239 We wondered whether the underwhelming response of the bystander S^- cell population could be
240 explained by a defect in paracrine communication between S^+ and S^- cells. Despite being present in high
241 abundance in S^+ cells as compared to mock-infected cells (table S1 and Fig. 2E), inflammatory cytokine
242 transcripts may not be translated. Indeed, initiation of translation seems to be impaired in SARS-CoV-
243 2 infected cells via two potential mechanisms: acceleration of cytosolic cellular mRNA degradation [20]
244 and blockade of the mRNA entry channel of ribosomes by the viral protein Nsp1 [45–47]. Moreover,
245 viral proteins Nsp8 and Nsp9 disrupt protein secretion in HEK293T cells [45], raising the possibility
246 that cytokines are produced but not secreted by S^+ cells.
247 To investigate these possibilities, we selected 5 inflammatory chemokines (IL-6, CXCL1, CCL2,
248 CXCL8/IL-8 and CCL20) whose expression was upregulated in S^+ cells upon infection (table S1) and

249 quantified their intracellular and secreted levels in lysates and supernatants of A549-ACE2 cells infected
250 for 24 hours (Fig. 3). As a comparison, A549-ACE2 cells transfected with the immuno-stimulant
251 poly(I:C) were included in the analysis. In a mixed population of S^+ and S^- cells, mRNAs of these 5
252 cytokines were significantly more abundant than in mock-infected cells (Fig. S3A), in agreement with
253 the increased levels of mRNAs detected in S^+ cells by RNA-seq (table S1). Their expression was also
254 induced by poly(I:C) (Fig. S3A). All five cytokines were expressed at detectable levels in cells
255 stimulated by viral infection or poly(I:C) (Fig. 3A), indicating that infection does not hamper the
256 translation of the corresponding mRNAs. As expected, based on their mRNA abundance (Fig. S3A),
257 intracellular levels of IL-6, CCL2 and CXCL8 significantly increased upon poly(I:C) stimulation as
258 compared to unstimulated control cells (Fig. 3A). By contrast, despite being induced by poly(I:C)
259 downstream signaling (Fig. S3A), CXCL1 and CCL20 levels were comparable in stimulated and
260 unstimulated cells (Fig. 3A). This could be due to a short protein half-life, protein degradation and/or
261 rapid secretion. Intracellular levels of CXCL1 increased significantly upon infection compared to mock-
262 infected cells (Fig. 3A) while intracellular levels of IL-6, CCL2, CXCL8 and CCL20 were similar in
263 both conditions. However, all 5 cytokines were significantly more secreted by infected cells than mock-
264 infected ones (Fig. 3B). Infected cells secreted even more IL-6 and CXCL1 than cells stimulated by
265 poly(I:C) (Fig. 3B). Thus, inflammatory cytokines are expressed and secreted by A549-ACE2 cells
266 infected with SARS-CoV-2, which is in line with the excessive inflammatory response reported in other
267 cellular models [19,21,24,26,39] and characteristic of severe cases of COVID-19 [4–6]. The absence of
268 paracrine communication that was revealed by the RNA-seq analysis of S^- cells (Fig. 1) is thus unlikely
269 to be linked to a defect in cytokine expression and secretion in S^+ cells.

270 Consistent with prior RNA-seq studies conducted in bulk A549-ACE2 cells [19,38,39], we failed
271 to observe a significant IFN-I and III signature in S^+ cells (table S1 and Fig. 2E), despite a robust
272 induction of NF-κB activity (Fig. 2E). To validate this further, we compared the level of IFNβ, IFN-λ1
273 and IFN-λ2/3 transcripts in A549-ACE2 cells infected for 24 hours. Cells treated with poly(I:C) were
274 used as positive controls for IFN production. Cells infected with Measles virus (MeV), a respiratory
275 RNA virus known to trigger an IFN response in A549 cells [48], were also included in the analysis for
276 comparison. Flow cytometry analysis identified on average 20 to 30% of cells positive for viral proteins
277 upon SARS-CoV-2 or MeV infection (Fig. 3C). As expected, the level of IFNβ, IFN-λ1 and IFN-λ2/3
278 transcripts increased in poly(I:C)-treated cells compared to cells exposed to the transfecting reagent
279 lipofectamine only (Fig. S3B). Amounts of IFNβ, IFN-λ1 and IFN-λ2/3 transcripts were several orders
280 of magnitude higher in MeV-infected cells than in SARS-CoV-2 infected cells (Fig. S3B). Consistently
281 with mRNA level analysis (Fig. S3B), around 200 and 850 pg/ml of IFNβ were secreted by MeV-
282 infected cells and poly(I:C)-treated cells, respectively (Fig. 3D). SARS-CoV-2 infected cells secreted
283 as little as 50 pg/ml of IFNβ, which was similar to the quantity secreted by mock-infected cells and
284 lipofectamine-exposed cells, likely representing baseline levels (Fig. 3D). MeV infected cells secreted
285 around 1000 pg/ml of IFN-λ1 and 5000 pg/ml of IFN-λ2/3 while no IFN-λ was detected in the

286 supernatant of SARS-CoV-2 infected cells (Fig. 3D). This baseline level of IFN type-I secretion and
287 absence of IFN type-III release by SARS-CoV-2-infected cells is likely to be responsible for the lack of
288 paracrine signaling revealed by the RNA-seq analysis (Fig. 1).
289
290 **Upregulated NF-κB target genes contribute to an optimal SARS-CoV-2 replication**
291 Numerous genes associated with the NF-κB signaling pathway fall into the category of genes that
292 escaped the virus-induced cellular shutoff (Fig. 2E). To determine which of these genes were directly
293 controlled by NF-κB, we cross-compared the upregulated genes with known NF-κB target genes.
294 Among the 68 upregulated NF-κB-targets in S^+ cells, we identified cytokines such as CXCL8/IL8 and
295 IL32 (Fig. 4A, S4A and table S5). NFKB1, which codes for the p105/p50 subunit of the transcription
296 factor, and is itself a NF-κB-target gene [49,50], also showed a significant transcriptional induction in
297 S^+ cells (Fig. 4A, S4A and S4B). Such mechanism generates an auto-regulatory feedback loop in the
298 NF-κB response [49]. To identify NF-κB-driven lncRNAs, we analyzed NF-κB chromatin
299 immunoprecipitation (ChIP)-sequencing data generated in A549 cells stimulated with TNF-α [51] and
300 searched for known NF-κB binding motifs [103]. The analysis recovered 15 NF-κB-targets among the
301 184 upregulated lncRNAs in S^+ cells (Fig 4A and table S5), including PACERR and ADIRF-AS1. In
302 U937 macrophages, PACERR modulates the expression of NF-κB-target genes *via* a direct interaction
303 with the NF-κB subunit p50 [52]. ADIRF-AS1 is an antisense lncRNA with no known function. Novel
304 NF-κB target genes were also identified among unannotated genes (Fig 4A and table S5).
305 Among the top upregulated NF-κB target genes identified in S^+ cells (Fig. 4A), we selected NFKB1,
306 CXCL8/IL8, IL32 and ADIRF-AS1 for functional analysis. NFKB1 served as a positive control in these
307 experiments since reducing its expression was previously shown to decrease SARS-CoV-2 protein
308 expression in A549-ACE2 cells [38]. These results were unexpected since NF-κB commonly acts as
309 antiviral factor [43]. Analysis of mRNA abundances showed a significant transcriptional induction of
310 NFKB1, CXCL8/IL8 and ADIRF-AS1 in a bulk population of A549-ACE2 cells infected by SARS-
311 CoV-2 for 24 hours, as compared to mock-infected cells (Fig. S4B), validating the RNA-seq analysis
312 performed on S^+ cells (Fig. 1). We had previously confirmed that IL32 transcripts were significantly
313 more abundant in S^+ cells than in mock-infected cells (Fig. 2C). We explored the potential ability of
314 NFKB1, CXCL8, IL32 and ADIRF-AS1 to modulate the replication of SARS-CoV-2 using siRNA-
315 mediated knock-down approaches. Twenty-four hours post-infection, intracellular viral RNA
316 production was quantified by RT-qPCR and the number of cells positive for the viral protein S was
317 assessed by flow cytometry analysis. RT-qPCR analyses revealed that the siRNA pools efficiently
318 reduced the expression of their respective targets in A549-ACE2 cells (Fig. 4B). Reduced expression of
319 NFKB1, CXCL8, IL32 and ADIRF-AS1 significantly decreased both the viral RNA yield and the
320 number of infected cells, as compared to cells transfected with control siRNA pools (Fig. 4C and 4D).
321 These results confirmed the pro-SARS-CoV-2 activity of NFKB1 in A459-ACE2 cells [38] and revealed
322 that CXCL8, IL32 and ADIRF-AS1 also exhibited significant proviral functions.

323 Thus, our sorting approaches identified coding and non-coding genes that contribute to an optimal
324 SARS-CoV-2 replication.
325
326 **Discussion**
327 Transcriptomic analysis of lung A549-ACE2 cells sorted based on Spike expression permitted deep
328 sequencing of many cells synchronized for viral protein expression. Depletion of viral RNA from the
329 samples prior to RNA-seq allowed for a robust identification of host cell DEGs. Our approach thus
330 unveiled an accurate and comprehensive picture of genome-wide signaling networks that are directly
331 affected by SARS-CoV-2 replication in human lung cells. It reveals a massive, but somehow selective,
332 gene expression shutoff in S^+ cells. Such reduction of cellular transcripts was underestimated in analysis
333 performed on bulk population of infected A549-ACE2 cells [19,38,39] but was detected by RNA-seq
334 analysis performed on bulk population of Calu-3 cells infected at an high MOI [20]. This is probably
335 due to the fact that Calu-3 cells express high levels of ACE2 [53] and are thus naturally permissive to
336 SARS-CoV-2, ensuring a high proportion of infected cells in the mixed culture. SARS-CoV-2 employs
337 several strategies to decrease the level of cellular mRNAs in infected cells, including inhibition of
338 nuclear mRNA export [20,45] and accelerated mRNA degradation as compared to control cells [20].
339 SARS and SARS-CoV-2 Nsp1 largely contribute to these processes by interacting with the mRNA
340 export machinery [54] and by inducing endonucleolytic cleavage of the 5′ UTR of capped mRNAs
341 bound to 40S ribosomes [20,55–57]. SARS-CoV-2 RNAs are protected from Nsp1-mediated
342 degradation by their 5' end leader sequence [20,58], which explains why we observed, in agreement
343 with previous studies performed in A549-ACE2 cells [19] and Calu-3 cells [20], a large dominance of
344 viral RNA over the cellular RNA pool at 24 hpi.
345 One consequence of this drastic shutoff is the suppression of expression of innate immune genes,
346 such as IFN type I and type III. In agreement with previous RNA-seq studies performed in bulk
347 population of infected A549-ACE2 cells [19,38] and kidney HEK293T-ACE2 cells [59], our
348 transcriptomic profiling combined with analysis of mRNA levels and IFN secretion showed that infected
349 cells failed to mount an antiviral response. Besides global gene expression reduction in host cells, SARS-
350 CoV-2 has evolved numerous mechanisms to specifically counteract the IFN induction and signaling
351 pathways [14]. For instance, the viral proteins Nsp6 and Nsp13 bind and block the ability of TANK
352 binding kinase 1 (TBK1) to phosphorylate IRF3 [13] and several viral proteins, including the N and
353 Orf6 proteins, dampen STAT1/2 phosphorylation or nuclear translocation [13,60,61]. Consistent with
354 an absence of IFN secretion by S^+ cells and, consequently, a poor paracrine response, the transcriptome
355 of bystander S- cells largely overlapped with the one of mock-infected cells. However, a small subset
356 of ISGs underwent modest transcriptional induction in bystander cells. They may be induced during an
357 early stage of viral replication, prior to the production of viral proteins that antagonize IFN signaling,
358 or by the minute amount of type I IFNs that was secreted by S^+ cells. Absence of IFN response is not,
359 however, a universal feature of SARS-CoV-2 infection. Viral replication induces a type I and III IFN

360 response in Calu-3 cells [62–65], primary airway epithelia cultured at the air-liquid interface [62,64],
361 human intestinal epithelial cells [66], organoid-derived bronchioalveolar models [67] and intestinal
362 organoids [68]. When infected at a high MOI, A549-ACE2 cells also induced expression of IFN and
363 ISGs [19]. Thus, in vitro, the magnitude of the IFN response elicited by SARS-CoV-2 is cell-type
364 specific and dependent on the viral load. Interestingly, RNA-seq analysis of postmortem lung tissues
365 from lethal cases of COVID-19 failed to detect IFN-I or IFN-III [19]. Type I IFN responses were highly
366 impaired in peripheral white blood cells of patients with severe or critical COVID-19, as indicated by
367 transcriptional analysis [18]. Moreover, infected patients had no detectable circulating IFN-β,
368 independently of the severity of the disease [18]. Thus, our results corroborate these clinical studies
369 highlighting the efficient shutdown of IFN production by the virus.

370 Although our RNA-seq analysis identified over 12000 host transcripts that were significantly
371 reduced during SARS-CoV-2 infection as compared to control cells, it also recovered around 1500
372 transcripts whose levels were significantly elevated and 2800 transcripts whose levels were unchanged
373 upon infection. Among top upregulated genes in S^+ cells, we identified numerous proinflammatory
374 cytokines, such as IL6, CXCL1, CCL2, IL8/CXCL8 and CCL20. ELISA analysis confirmed that
375 infected cells were producing these inflammatory cytokines. They were previously identified in bulk or
376 sc-RNA analysis of A549-ACE2 cells as upregulated [19,38,39], while others, such as IL32, were
377 underreported. High levels of proinflammatory cytokine transcripts have been also reported in infected
378 primary bronchial cells [19], in lung macrophages [27] and post-mortem lung samples of COVID-19-
379 positive patients [19]. Thus, SARS-CoV-2 appears to selectively inhibit IFN signaling while allowing
380 chemokine production in lung cells.

381 GO and KEGG pathway analyses confirmed the upregulation of an inflammatory response in S^+
382 cells, including TNF- and NF-κB- transcriptional signatures. An NF-κB transcriptional footprint was
383 previously identified in RNA-seq analysis of bulk population of SARS-CoV-2-infected tracheal-
384 bronchial epithelial cells [26] and in scRNA-seq analysis of infected A549-ACE2 cells [38]. Microarray
385 analysis of Calu-3 cells infected with SARS-CoV-2 also showed a specific bias towards an NF-κB
386 mediated inflammatory response [39]. Finally, inflammatory genes specifically up-regulated in
387 peripheral blood immune cells of severe patients or critical COVID-19 patients mainly belonged to the
388 NF-κB pathway [18]. Consistently, among the 741 upregulated protein-coding genes that we identified
389 in S^+ cells, 68 possess an NF-κB binding site in their promoter regions. Examples include IL6,
390 CXCL8/IL8 and IL32. We also identified NF-κB binding site in the promoter regions of lncRNAs that
391 were upregulated in S^+ cells, such as ADIRF-AS1 and PACERR. NF-κB contribution to the antiviral
392 response is well described and is supported by numerous in vivo experiments showing that mice
393 deficient in different NF-κB subunits are more susceptible to viral infection than wild-type mice [43].
394 Consistently, many viruses have evolved strategies to counteract the NF-κB-mediated antiviral response
395 [69]. However, certain human viruses, such as HIV-1, Epstein-Barr virus and influenza A virus, activate
396 NF-κB to block apoptosis and prolong survival of the host cell to gain time for replication [70]. Our data

397 show that disruption of NF-κB function through silencing of its subunit p105/p50 diminished the
398 production of viral RNAs and proteins at 24 hpi in A549-ACE2 cells, confirming its proviral role
399 [38,39]. Several SARS-CoV-2 proteins could contribute to the activation of NF-κB signaling in infected
400 cells. When individually expressed, Orf7a and Nsp14 activate NF-κB signaling pathway and induce
401 cytokine expression, in Hela and HEK293T cells, respectively [71,72]. Nsp5 also induces the expression
402 of several inflammatory cytokines, such as IL-6 and TNF-α, through activation of NF-κB in Calu-3 and
403 THP1 cells [73]. Further studies are required to understand how SARS-CoV-2 benefits from hijacking
404 NF-κB-driven functions.

405 Consistent with a proviral role of NF-κB in the context of SARS-CoV-2 infection, we found that
406 diminished expression of three NF-κB target genes (IL32, CXCL8/IL8, and ADIRF-AS1) significantly
407 decreased viral RNA and protein production. IL32 is a proinflammatory interleukin secreted by immune
408 and non-immune cells that induces the expression of other inflammatory cytokines, including TNF-*α*,
409 IL6, and IL1*β* [74]. IL32 was previously described as an antiviral factor in the context of infection with
410 several RNA and DNA viruses. For instance, its secretory isoform reduces the replication of Hepatitis
411 B virus by stimulating the expression of IFN-λ1 [75]. Its antiviral activity was also demonstrated in U1
412 macrophages infected with HIV-1 [76] and canine kidney cells infected with influenza A [77], using
413 silencing and over-expression approaches, respectively. Further studies are required to understand the
414 pro-SARS-CoV-2 function of endogenous IL32. It may support SARS-CoV-2 replication *via* its ability
415 to activate NF-κB [78]. CXCL8/IL8 is a potent neutrophil chemotactic factor. It was previously shown
416 to possess proviral functions in the context of infection by several unrelated RNA and DNA viruses,
417 probably via inhibition of the antiviral action of IFN-α [79,80]. It could act in a similar manner in SARS-
418 CoV-2 infected A549-ACE2 cells.

419 As for coding genes, there was a higher proportion of down- *versus* up-regulated lncRNAs in S^+
420 cells. GO cannot be extrapolated from lncRNAs since most of them have no known function, indicating
421 the need for future studies in this area. Several RNA-seq and microarray studies have identified hundreds
422 of lncRNAs induced by IFN stimulation or viral infection in diverse human and mice cell types [35,81–
423 83]. Analysis of a handful of them has provided a glimpse of the potential regulatory impact of this class
424 of RNAs on the IFN response itself [84] and on ISG expression [35,81,83]. However, the investigation
425 of the precise role of individual lncRNAs in IFN-mediated antiviral response is still in its infancy stage.
426 By analyzing publicly available SARS-CoV-2-infected transcriptome data, several studies recovered
427 lncRNAs that were misregulated upon infection of human lung epithelial cell lines, primary normal
428 human bronchial epithelial cells and BALF [85–88]. However, no lncRNA with a direct action on the
429 life cycle of SARS-CoV-2 has been identified prior to this study. We show that the lncRNA ADIRF-
430 AS1, which was among the top upregulated lncRNAs both in S^+ cells and in a dataset that we re-analyzed
431 [19], has a proviral function. We identified a NF-κB binding site near its promoter region. It would be
432 interesting to understand the mechanisms by which ADIRF-AS1 enhances SARS-CoV-2 replication and
433 whether its proviral function depends on NF-κB.

434 Finally, our analysis profiled about 600 differentially expressed unannotated polyA+ transcripts in
435 S+ and bystander cells. The identification of these unannotated genes confirms that the genome is far
436 from being well characterized. Having specific RNAs expressed in particular conditions could open the
437 way for the identification of pro- or anti-viral genes that could be used for better prognosis of at-risk
438 patients or for the follow up of the disease severity.
439 Our data suggests that the genes that are refractory to the viral-induced shutoff are proviral genes.
440 Understanding the molecular mechanisms underlying the selectivity of the shut-off would be interesting.
441 Since coronavirus Nsp1 induces the cleavage of the 5'UTR of capped transcripts bound to 40S
442 ribosomes, the 5'UTR length and/or structure may affect Nsp1 binding and subsequent degradation.
443 Alternatively, the extent of transcript reduction may be linked to their GC content and/or their lengths,
444 which could affect the specificity of the host RNase that is presumably recruited by Nsp1. Discovering
445 the host RNase responsible for transcript degradation in SARS-CoV-2-infected cells will shed light on
446 the mechanism of selectivity of the viral-induced shutoff.
447
448 **Material and Methods**
449 **Cell lines.** Human lung epithelial A549-ACE2 cells, which have been modified to stably express
450 ACE2 *via* lentiviral transduction, were generated in the laboratory of Pr. Olivier Schwartz (Institut
451 Pasteur, Paris, France). A549-ACE2 and African green monkey Vero E6 cells (ATCC CRL-1586) were
452 cultured in high-glucose DMEM media (Gibco), supplemented with 10% fetal bovine serum (FBS;
453 Sigma) and 1% penicillin-streptomycin (P/S; Gibco). Cells were maintained at 37°C in a humidified
454 atmosphere with 5% CO_2.
455 **Virus and infections.** Experiments with SARS-CoV-2 isolates were performed in a BSL-3
456 laboratory, following safety and security protocols approved by the risk prevention service of Institut
457 Pasteur. The strain BetaCoV/France/IDF0372/2020 was supplied by the National Reference Centre for
458 Respiratory Viruses hosted by Institut Pasteur (Paris, France) and headed by Pr. S. van Der Werf. The
459 human sample from which the strain was isolated has been provided by Dr. X. Lescure and Pr. Y.
460 Yazdanpanah from the Bichat Hospital, Paris, France. Viral stocks were produced by amplification on
461 Vero E6 cells, for 72 h in DMEM 2% FBS. The cleared supernatant was stored at 80°C and titrated on
462 Vero E6 cells by using standard plaque assays to measure plaque-forming units per ml (PFU/ml). A549-
463 ACE2 were infected at MOI of 1 in DMEM without FBS. After 2 h, DMEM with 5% FBS was added
464 to the cells. The Measles Schwarz strain expressing GFP (MeV-GFP) was described previously [89]
465 and was used at an MOI of 1.
466 **Poly I:C stimulation.** Cells were stimulated with 10 ng/µL Poly(I:C) (HMW, #vac-pic Invivogen)
467 using Lipofectamine 3000 Reagent (Thermo Fisher Scientific) according to manufacturer's protocol.
468 Treatment was maintained for 24 hours, concomitantly with infection.
469 **Flow cytometry.** Cells were detached with trypsin, washed with PBS and fixed in 4% PFA for 30
470 min at 4°C. Intracellular staining was performed in PBS, 2% BSA, 2mM EDTA and 0.1% Saponin

471 (FACS buffer). Cells were incubated with antibodies recognizing the spike protein of SARS-CoV-2
472 (anti-S2 H2 162, a kind gift from Dr. Hugo Mouquet, Institut Pasteur, Paris, France) and subsequently
473 with secondary anti-human AlexaFluor-647 antibody (1:1000, A21455 Thermo) for 30 min at 4°C. Data
474 were acquired using Attune NxT Acoustic Focusing Cytometer (Thermo Fisher) and analyzed using
475 FlowJo software.

476 **SARS-CoV-2 infected and bystander cell-sorting and RNA extraction on fixed samples for**
477 **RNA-seq.** A549-ACE2 cells were seeded the day prior to infection. Cells were infected with SARS-
478 CoV-2 at MOI 1 or mock infected. Infections were done in two independent repeats with three technical
479 replicates each. At 24 h post infection, cells were detached with trypsin, fixed in 4% PFA for 30 min on
480 ice and stained for spike protein as described above for flow cytometry, with RNasin added to FACS
481 buffer (1:100 dilution) just before use to prevent RNA degradation. Infected cell samples were
482 resuspended in PBS 2%, 25 mM Hepes, 5 mM EDTA (sorting buffer) and sorted at 4°C on a FACSAria
483 Fusion4L Sorter into infected (presence of S protein expression) and bystander (absence of viral protein
484 expression) cell populations. Cells were collected in FBS-coated tubes containing buffer with RNasin
485 to minimize RNA degradation. After sorting, cells were pelleted at 500g for 5 min at 4°C and RNA was
486 extracted with the RecoverAll Total Nucleic Acid Isolation Kit starting at the protease digestion step.
487 Digestion was performed for 15 min at 50°C and 15 min at 80°C in the presence of RNasin. Extraction
488 was performed according to manufacturer's instructions and the addition of RNAsin to all buffers just
489 before use until final elution of RNA in DNAse-free water. Residual DNA was further digested using
490 DNAse I (Invitrogen AM1906). RNAs were sorted at -80°C until further analysis.

491 **Library preparation, viral RNA depletion and RNA-sequencing.** 500-1000 ng of total RNA
492 were depleted of SARS-CoV-2 RNA using custom designed probes. The probes were synthesized using
493 the NC_045512.2 Wuhan-Hu-1 complete genome reference. The design was made by Illumina and is
494 composed of 459 probes, separated into two pools synthetized by IDT. For the SARS-CoV-2 depletion,
495 we mixed both pools and used 1µl of this mix per sample, replacing the Ribozero+ probes at the
496 ribodepletion reaction step of the Illumina Stranded Total RNA prep ligation protocol. The SARS-CoV-
497 2 depleted RNA samples were normalized to 300ng and ERCC Spike was added as recommended by
498 the protocol ERCC RNA Spike-In Control mixes User Guide. The libraries were prepared using the
499 Illumina Stranded mRNA Prep Ligation Reference Guide.

500 **PolyA+ RNA-sequencing analysis of sorted cells.** Dataset consists of 9 paired-end libraries (150
501 nt), 3 replicates per condition: mock, bystander and infected cells. Adaptors were trimmed with Trim
502 Galore v0.6.4 [90] (wrapper for cutadapt v2.10 [91] and FastQC v0.11.9 [92]), with options --stringency
503 5 --trim-n -q 20 --length 20 --paired --retain_unpaired. Reads were mapped to a reference containing
504 human genome (hg38), SARS-CoV-2 (NC045512.2) and ERCC sequences. STAR v2.7.3a [93] was
505 used to map the reads, with default parameters. Bam files were then filtered using SAMtools v1.10 [94]
506 to retained reads flagged as primary alignment, and with mapping quality > 30 (option -q 30 -F 0x100 -
507 F 0x800). Read coverage was computed for each strand with bamCoverage (deepTools v3.5.0 [95]) with

508 options --binSize 1 --skipNAs --filterRNAstrand forward/reverse. For the detection of unannotated
509 transcripts, Scallop v0.10.5 [36] was used to reconstruct transcripts, with options --library_type first --
510 min_transcript_coverage 2 --min_splice_bundary_hits 5 --min_flank_length 5. Scallop was run on each
511 library, and the resulting annotations were merged using cuffmerge v1.0.0 [96], with gencode annotation
512 (v32) as reference (-g option). Then BEDtools v2.29.2 [97] was used to retain only intergenic and
513 antisens transcripts regarding gencode annotation. Gene expression quantification was performed using
514 featureCounts v2.0.0 [98], with options -O -M --fraction -s 2 -p, using a merged annotation of gencode
515 v32, SARS-CoV-2 (NC045512.2), newly annotated transcripts and ERCC transcripts. Subsequent
516 analyses were performed in R v3.6.2 [99]. Differential expression analysis was performed using DESeq2
517 package [100], after filtering out genes with less than 10 raw counts for all replicates in at least one
518 condition. Gene counts were normalized on ERCC counts, using *estimateSizeFactorsForMatrix*
519 function from DESeq2. All pairwise comparisons were performed (mock vs infected, mock vs bystander
520 and bystander vs infected), and genes were retained as differential if adjusted p-value was < 0.05 and
521 log fold-change > 1 or < -1. All plots were made using custom script, except for heatmaps that were
522 done using pheatmap package (RRID:SCR_016418).

523 **PolyA+ RNA-sequencing analysis of bulk population of infected cells (from a public dataset).**
524 Fastq files produced in the study of Blanco-Melo et al (2020)[19] were retrieved from GEO repository
525 (GSE147507). Dataset consist of single-end libraries (150 nt). We compared A549-ACE2 "mock" cells
526 (SRR11517680, SRR11517681 & SRR11517682) *versus* A549-ACE2 cells infected with SARS-CoV-
527 2 at MOI 0.2 (SRR11517741, SRR11517742 & SRR11517743). Adaptors were trimmed with Trim
528 Galore v0.6.4 [90], with options --stringency 5 --trim-n -q 20 --length 20. Reads were mapped on a
529 reference containing human genome (hg38) and SARS-CoV-2 (NC045512.2) sequence. Bam files were
530 then filtered using SAMtools v1.10 [94] to retained reads flagged as primary alignment, and with
531 mapping quality > 30 (option -q 30 -F 0x100 -F 0x800). Gene expression quantification was performed
532 using featureCounts v2.0.0 [98], with options -O -M --fraction -s 2, using a merged annotation of
533 gencode v32, SARS-CoV-2 (NC045512.2) and newly annotated transcripts. Gene counts were
534 normalized on the full count matrix, using *estimateSizeFactorsForMatrix* function from DESeq2 [100].
535 Differential analysis was performed as described above.

536 **GO enrichment analysis.** The GO enrichment and KEGG pathway analysis were performed using
537 DAVID online tool (updated version 2021) [101,102]. Upregulated protein-coding genes from each
538 comparison were taken for the analysis with default background for *Homo sapiens*.
539 GOTERM_BP_DIRECT and KEGG pathway were retained and top 10 results based on adjusted p-
540 value (Benjamini) were plotted using ggplot2 R package (v 3.3.0).

541 **Identification of NF-κB target genes.** A list of coding genes that are known targets of NF-kB is
542 available on Gilmore's laboratory website (https://www.bu.edu/nf-kb/gene-resources/target-genes). We
543 selected genes from this list that were shown to be direct targets of NF-κB, and for which the gene
544 symbol could be retrieved in gencode annotation (354 genes). For identifying lncRNAs and

545 unreferenced RNAs that possess NF-κB binding site in their promoter, we used p65 ChIP-seq data from
546 GEO dataset GSE34329 [51] - one input file and 2 ChIP replicates, 38nt long reads, single-end. Reads
547 were mapped using bowtie2 v2.4.1 using hg38 as reference, and SAMtools was used to retained the one
548 flagged as primary alignment, with mapping quality > 30, and to remove PCR duplicates (markdup,
549 with -r option). NF-κB binding sites were then detected using macs2 v2.2.7.1 [103], with command
550 callpeak -t ChIP_BamFile1 ChIP_BamFile2 -c input_BamFile -f BAM -g hs -s 38 --keep-dup all. Peaks
551 in the first decile of the -log10(qvalue) value were discarded. NF-kB motif genomic coordinates in the
552 human genome were retrieved using EMBOSS fuzznuc v6.6 [104], using motif 5'-
553 G(3)[AG]N[CT](3)C(2) - 3' [105], on forward and reverse strand (option -complement Y). Peaks and
554 NF-κB motif coordinates were compared using BEDtools [97]; if a motif was contained in a peak, the
555 motif strand was assigned to the peak. LncRNA and un-references transcripts were identified as NF-κB
556 potential targets if their promoter region (1kb before transcript TSS) had a peak containing a motif or a
557 peak for which the -log10(qvalue) was in the top 5%.

558 **RNA extraction and RT-qPCR assays.** Total RNA was extracted from cells with the NucleoSpin
559 RNA II kit (Macherey-Nagel) according to the manufacturer's instructions. First-strand complementary
560 DNA (cDNA) synthesis was performed with the RevertAid H Minus M-MuLV Reverse Transcriptase
561 (Thermo Fisher Scientific) using random primers. Quantitative real-time PCR was performed on a real-
562 time PCR system (QuantStudio 6 Flex, Applied Biosystems) with Power SYBR Green RNA-to-CT 1-
563 Step Kit (Thermo Fisher Scientific). Data were analyzed using the 2-ΔΔCT method, with all samples
564 normalized to endogenous BPTF, whose gene expression was confirmed as homogenous across samples
565 by RNA-seq. Genome equivalent concentrations were determined by extrapolation from a standard
566 curve generated from serial dilutions of plasmid encoding a fragment of the RNA-dependent RNA
567 polymerase (RdRp)-IP4 of SARS-CoV-2. Primers used for RT-qPCR analysis are given in table S6.

568 **siRNA-mediated knockdown.** A549-ACE2 cells were transfected using Lipofectamine RNAiMax
569 (Life Technologies) with 10nM of control (#4390843, Ambion) or CXCL8 (L-004756-00, Dharmacon),
570 NFKB1 (L-003520-00, Dharmacon), IL32 (L-015988-00, Dharmacon), ADIRF-AS1 (siTOOLs
571 Biotech) siRNAs following the manufacturer's instructions. 48h after transfection, cells were infected
572 with SARS-CoV-2 for 24 h.

573 **Chemokine and Interferon expression and secretion.** Cell lysates for intracellular chemokine
574 quantification were obtained *via* repeated freeze-thaw cycles at -80°C of cells suspended in media
575 containing protease inhibitor cocktail (Roche Applied Science) and final centrifugation at 8000g to
576 pellet debris. IL6, CXCL1, CCL2, CXCL8 and CCL20 concentrations in supernatants of from control,
577 infected or stimulated cells, were measured using a custom-designed LEGENDplex Human Panel. Data
578 were acquired on an Attune NxT Flow Cytometer (Thermo Fisher) analyzed with LEGENDplex
579 software (BioLegend). Similarly, IFN-β, IFN-λ1 and IFN- λ2/3 concentrations were measured in
580 undiluted supernatants from control, infected or stimulated cells using a LEGENDplex Human Type
581 1/2/3 Interferon Panel assay (BioLegend) according to the manufacturer's protocol.

Statistical analysis. Statistical parameters including the exact value of n, precision measures (as means ± SEM), statistical tests and statistical significance are reported in the figure legends. In figures, asterisks denote statistical significance: *p < 0.05, **p < 0.01, ***p < 0.005, ****p < 0.0001, and "ns" indicates not significant. Statistical analysis was performed in GraphPad Prism 9 (GraphPad Software Inc.).

Acknowledgments

We thank the French National Reference Centre for Respiratory Viruses hosted by Institut Pasteur (France) and headed by Pr. S. van Der Werf for providing the historical SARS-CoV-2 strain; C. Combredet and F. Tangy (Institut Pasteur) for producing and sharing MeV-GFP; H. Mouquet and C. Planchais (Institut Pasteur) for anti-S antibodies and O. Schwartz (Institut Pasteur) for the A549-ACE2 cells. We are grateful to our team member Felix Streicher for helping design the figure 2A and to all members of our laboratories for helpful discussions. We acknowledge the UTechS Immunology Platform of Institut Pasteur for the use of the cell sorter. The Biomics Platform was supported by France Génomique (ANR-10-INBS-09), IBISA and the Illumina COVID-19 Projects' offer.

Funding

This work was funded by the CNRS (NJ), Institut Pasteur (NJ), 'Urgence COVID-19' fundraising campaign of Institut Pasteur (NJ), ANR-DARK COVID (AM/NJ) and DIM-1-Health (NJ/AM). DF postdoctoral fellowship was supported by the DIM-1-Health from the Conseil Régional d'Ile-de-France. SMA is supported by the Pasteur-Paris University (PPU) International PhD Program. The funders had no role in study design, data collection and analysis, decision to publish or preparation of the manuscript.

References

609 1. Wiersinga WJ, Rhodes A, Cheng AC, Peacock SJ, Prescott HC. Pathophysiology,
610 Transmission, Diagnosis, and Treatment of Coronavirus Disease 2019 (COVID-19): A
611 Review. JAMA. 2020;324: 782–793. doi:10.1001/jama.2020.12839
612 2. Trypsteen W, Cleemput JV, Snippenberg W van, Gerlo S, Vandekerckhove L. On the
613 whereabouts of SARS-CoV-2 in the human body: A systematic review. PLOS Pathogens.
614 2020;16: e1009037. doi:10.1371/journal.ppat.1009037
615 3. Pedersen SF, Ho Y-C. SARS-CoV-2: a storm is raging. J Clin Invest. 2020;130: 2202–
616 2205. doi:10.1172/JCI137647
617 4. Chen G, Wu D, Guo W, Cao Y, Huang D, Wang H, et al. Clinical and immunological
618 features of severe and moderate coronavirus disease 2019. J Clin Invest. 2020;130: 2620–
619 2629. doi:10.1172/JCI137244
620 5. Lucas C, Wong P, Klein J, Castro TBR, Silva J, Sundaram M, et al. Longitudinal
621 analyses reveal immunological misfiring in severe COVID-19. Nature. 2020;584: 463–469.
622 doi:10.1038/s41586-020-2588-y
623 6. Giamarellos-Bourboulis EJ, Netea MG, Rovina N, Akinosoglou K, Antoniadou A,
624 Antonakos N, et al. Complex Immune Dysregulation in COVID-19 Patients with Severe
625 Respiratory Failure. Cell Host Microbe. 2020;27: 992-1000.e3.
626 doi:10.1016/j.chom.2020.04.009
627 7. Chen L, Deng H, Cui H, Fang J, Zuo Z, Deng J, et al. Inflammatory responses and
628 inflammation-associated diseases in organs. Oncotarget. 2017;9: 7204–7218.
629 doi:10.18632/oncotarget.23208
630 8. Jouvenet N, Goujon C, Banerjee A. Clash of the titans: interferons and SARS-CoV-2.
631 Trends Immunol. 2021;42: 1069–1072. doi:10.1016/j.it.2021.10.009
632 9. Streicher F, Jouvenet N. Stimulation of Innate Immunity by Host and Viral RNAs.
633 Trends in Immunology. 2019;40: 1134–1148. doi:10.1016/j.it.2019.10.009
634 10. Schneider WM, Chevillotte MD, Rice CM. Interferon-Stimulated Genes: A Complex
635 Web of Host Defenses. Annu Rev Immunol. 2014;32: 513–545. doi:10.1146/annurev-
636 immunol-032713-120231
637 11. Schoggins JW. Recent advances in antiviral interferon-stimulated gene biology.
638 F1000Res. 2018;7: 309. doi:10.12688/f1000research.12450.1
639 12. Katze MG, He Y, Gale M. Viruses and interferon: a fight for supremacy. Nat Rev
640 Immunol. 2002;2: 675–687. doi:10.1038/nri888
641 13. Xia H, Cao Z, Xie X, Zhang X, Chen JY-C, Wang H, et al. Evasion of Type I
642 Interferon by SARS-CoV-2. Cell Rep. 2020;33: 108234. doi:10.1016/j.celrep.2020.108234
643 14. Beyer DK, Forero A. Mechanisms of Antiviral Immune Evasion of SARS-CoV-2. J
644 Mol Biol. 2021; 167265. doi:10.1016/j.jmb.2021.167265
645 15. Sa Ribero M, Jouvenet N, Dreux M, Nisole S. Interplay between SARS-CoV-2 and
646 the type I interferon response. PLoS Pathog. 2020;16: e1008737.
647 doi:10.1371/journal.ppat.1008737
648 16. Singh M, Chazal M, Quarato P, Bourdon L, Malabat C, Vallet T, et al. A virus-derived
649 microRNA targets immune response genes during SARS-CoV-2 infection. EMBO Rep. 2021;
650 e54341. doi:10.15252/embr.202154341
651 17. Pawlica P, Yario TA, White S, Wang J, Moss WN, Hui P, et al. SARS-CoV-2
652 expresses a microRNA-like small RNA able to selectively repress host genes. PNAS.
653 2021;118. doi:10.1073/pnas.2116668118
654 18. Hadjadj J, Yatim N, Barnabei L, Corneau A, Boussier J, Smith N, et al. Impaired type
655 I interferon activity and inflammatory responses in severe COVID-19 patients. Science.
656 2020;369: 718–724. doi:10.1126/science.abc6027
657 19. Blanco-Melo D, Nilsson-Payant BE, Liu W-C, Uhl S, Hoagland D, Møller R, et al.
658 Imbalanced Host Response to SARS-CoV-2 Drives Development of COVID-19. Cell.

659 2020;181: 1036-1045.e9. doi:10.1016/j.cell.2020.04.026
660 20. Finkel Y, Gluck A, Nachshon A, Winkler R, Fisher T, Rozman B, et al. SARS-CoV-2
661 uses a multipronged strategy to impede host protein synthesis. Nature. 2021;594: 240–245.
662 doi:10.1038/s41586-021-03610-3
663 21. Wyler E, Mösbauer K, Franke V, Diag A, Gottula LT, Arsiè R, et al. Transcriptomic
664 profiling of SARS-CoV-2 infected human cell lines identifies HSP90 as target for COVID-19
665 therapy. iScience. 2021;24: 102151. doi:10.1016/j.isci.2021.102151
666 22. Xiong Y, Liu Y, Cao L, Wang D, Guo M, Jiang A, et al. Transcriptomic
667 characteristics of bronchoalveolar lavage fluid and peripheral blood mononuclear cells in
668 COVID-19 patients. Emerg Microbes Infect. 2020;9: 761–770.
669 doi:10.1080/22221751.2020.1747363
670 23. Carlin AF, Vizcarra EA, Branche E, Viramontes KM, Suarez-Amaran L, Ley K, et al.
671 Deconvolution of pro- and antiviral genomic responses in Zika virus-infected and bystander
672 macrophages. Proc Natl Acad Sci U S A. 2018;115: E9172–E9181.
673 doi:10.1073/pnas.1807690115
674 24. Triana S, Metz-Zumaran C, Ramirez C, Kee C, Doldan P, Shahraz M, et al. Single-cell
675 analyses reveal SARS-CoV-2 interference with intrinsic immune response in the human gut.
676 Molecular Systems Biology. 2021;17: e10232. doi:10.15252/msb.202110232
677 25. Fiege JK, Thiede JM, Nanda HA, Matchett WE, Moore PJ, Montanari NR, et al.
678 Single cell resolution of SARS-CoV-2 tropism, antiviral responses, and susceptibility to
679 therapies in primary human airway epithelium. PLoS Pathog. 2021;17: e1009292.
680 doi:10.1371/journal.ppat.1009292
681 26. Ravindra NG, Alfajaro MM, Gasque V, Huston NC, Wan H, Szigeti-Buck K, et al.
682 Single-cell longitudinal analysis of SARS-CoV-2 infection in human airway epithelium
683 identifies target cells, alterations in gene expression, and cell state changes. PLOS Biology.
684 2021;19: e3001143. doi:10.1371/journal.pbio.3001143
685 27. Liao M, Liu Y, Yuan J, Wen Y, Xu G, Zhao J, et al. Single-cell landscape of
686 bronchoalveolar immune cells in patients with COVID-19. Nat Med. 2020;26: 842–844.
687 doi:10.1038/s41591-020-0901-9
688 28. Chen G, Ning B, Shi T. Single-Cell RNA-Seq Technologies and Related
689 Computational Data Analysis. Front Genet. 2019;10: 317. doi:10.3389/fgene.2019.00317
690 29. Zhang MJ, Ntranos V, Tse D. Determining sequencing depth in a single-cell RNA-seq
691 experiment. Nat Commun. 2020;11: 774. doi:10.1038/s41467-020-14482-y
692 30. Kopp F, Mendell JT. Functional Classification and Experimental Dissection of Long
693 Noncoding RNAs. Cell. 2018;172: 393–407. doi:10.1016/j.cell.2018.01.011
694 31. Iyer MK, Niknafs YS, Malik R, Singhal U, Sahu A, Hosono Y, et al. The landscape of
695 long noncoding RNAs in the human transcriptome. Nat Genet. 2015;47: 199–208.
696 doi:10.1038/ng.3192
697 32. Encode Project Consortium. An integrated encyclopedia of DNA elements in the
698 human genome. Nature. 2012;489: 57–74. doi:10.1038/nature11247
699 33. Guttman M, Amit I, Garber M, French C, Lin MF, Feldser D, et al. Chromatin
700 signature reveals over a thousand highly conserved large non-coding RNAs in mammals.
701 Nature. 2009;458: 223–7. doi:10.1038/nature07672
702 34. Meng XY, Luo Y, Anwar MN, Sun Y, Gao Y, Zhang H, et al. Long Non-Coding
703 RNAs: Emerging and Versatile Regulators in Host-Virus Interactions. Front Immunol.
704 2017;8: 1663. doi:10.3389/fimmu.2017.01663
705 35. Carnero E, Barriocanal M, Segura V, Guruceaga E, Prior C, Borner K, et al. Type I
706 Interferon Regulates the Expression of Long Non-Coding RNAs. Front Immunol. 2014;5:
707 548. doi:10.3389/fimmu.2014.00548
708 36. Shao M, Kingsford C. Accurate assembly of transcripts through phase-preserving

709 graph decomposition. Nat Biotechnol. 2017;35: 1167–1169. doi:10.1038/nbt.4020
710 37. Morillon A, Gautheret D. Bridging the gap between reference and real transcriptomes.
711 Genome Biology. 2019;20: 112. doi:10.1186/s13059-019-1710-7
712 38. Nilsson-Payant BE, Uhl S, Grimont A, Doane AS, Cohen P, Patel RS, et al. The NF-
713 κB Transcriptional Footprint Is Essential for SARS-CoV-2 Replication. J Virol. 2021;95:
714 e0125721. doi:10.1128/JVI.01257-21
715 39. Neufeldt CJ, Cerikan B, Cortese M, Frankish J, Lee J-Y, Plociennikowska A, et al.
716 SARS-CoV-2 infection induces a pro-inflammatory cytokine response through cGAS-STING
717 and NF-κB. Commun Biol. 2022;5: 1–15. doi:10.1038/s42003-021-02983-5
718 40. Herter EK, Li D, Toma MA, Vij M, Li X, Visscher D, et al. WAKMAR2, a Long
719 Noncoding RNA Downregulated in Human Chronic Wounds, Modulates Keratinocyte
720 Motility and Production of Inflammatory Chemokines. Journal of Investigative Dermatology.
721 2019;139: 1373–1384. doi:10.1016/j.jid.2018.11.033
722 41. Zhu X, Liu Y, Yu J, Du J, Guo R, Feng Y, et al. LncRNA HOXA-AS2 represses
723 endothelium inflammation by regulating the activity of NF-κB signaling. Atherosclerosis.
724 2019;281: 38–46. doi:10.1016/j.atherosclerosis.2018.12.012
725 42. Liu B, Sun L, Liu Q, Gong C, Yao Y, Lv X, et al. A Cytoplasmic NF-κB Interacting
726 Long Noncoding RNA Blocks IκB Phosphorylation and Suppresses Breast Cancer Metastasis.
727 Cancer Cell. 2015;27: 370–381. doi:10.1016/j.ccell.2015.02.004
728 43. Santoro MG, Rossi A, Amici C. NF-kappaB and virus infection: who controls whom.
729 EMBO J. 2003;22: 2552–2560. doi:10.1093/emboj/cdg267
730 44. Aggarwal BB. Signalling pathways of the TNF superfamily: a double-edged sword.
731 Nat Rev Immunol. 2003;3: 745–756. doi:10.1038/nri1184
732 45. Banerjee AK, Blanco MR, Bruce EA, Honson DD, Chen LM, Chow A, et al. SARS-
733 CoV-2 Disrupts Splicing, Translation, and Protein Trafficking to Suppress Host Defenses.
734 Cell. 2020;183: 1325-1339.e21. doi:10.1016/j.cell.2020.10.004
735 46. Lapointe CP, Grosely R, Johnson AG, Wang J, Fernández IS, Puglisi JD. Dynamic
736 competition between SARS-CoV-2 NSP1 and mRNA on the human ribosome inhibits
737 translation initiation. Proc Natl Acad Sci U S A. 2021;118: e2017715118.
738 doi:10.1073/pnas.2017715118
739 47. Yuan S, Peng L, Park JJ, Hu Y, Devarkar SC, Dong MB, et al. Nonstructural Protein 1
740 of SARS-CoV-2 Is a Potent Pathogenicity Factor Redirecting Host Protein Synthesis
741 Machinery toward Viral RNA. Mol Cell. 2020;80: 1055-1066.e6.
742 doi:10.1016/j.molcel.2020.10.034
743 48. Helin E, Vainionpää R, Hyypiä T, Julkunen I, Matikainen S. Measles virus activates
744 NF-kappa B and STAT transcription factors and production of IFN-alpha/beta and IL-6 in the
745 human lung epithelial cell line A549. Virology. 2001;290: 1–10. doi:10.1006/viro.2001.1174
746 49. Oeckinghaus A, Ghosh S. The NF-κB Family of Transcription Factors and Its
747 Regulation. Cold Spring Harb Perspect Biol. 2009;1: a000034.
748 doi:10.1101/cshperspect.a000034
749 50. Ten RM, Paya CV, Israël N, Le Bail O, Mattei MG, Virelizier JL, et al. The
750 characterization of the promoter of the gene encoding the p50 subunit of NF-kappa B
751 indicates that it participates in its own regulation. EMBO J. 1992;11: 195–203.
752 51. Raskatov JA, Meier JL, Puckett JW, Yang F, Ramakrishnan P, Dervan PB.
753 Modulation of NF-κB-dependent gene transcription using programmable DNA minor groove
754 binders. Proc Natl Acad Sci U S A. 2012;109: 1023–1028. doi:10.1073/pnas.1118506109
755 52. Krawczyk M, Emerson BM. p50-associated COX-2 extragenic RNA (PACER)
756 activates COX-2 gene expression by occluding repressive NF-κB complexes. Elife. 2014;3:
757 e01776. doi:10.7554/eLife.01776
758 53. Murgolo N, Therien AG, Howell B, Klein D, Koeplinger K, Lieberman LA, et al.

759 SARS-CoV-2 tropism, entry, replication, and propagation: Considerations for drug discovery
760 and development. PLOS Pathogens. 2021;17: e1009225. doi:10.1371/journal.ppat.1009225
761 54. Zhang K, Miorin L, Makio T, Dehghan I, Gao S, Xie Y, et al. Nsp1 protein of SARS-
762 CoV-2 disrupts the mRNA export machinery to inhibit host gene expression. Science
763 Advances. 2021 [cited 6 Feb 2022]. doi:10.1126/sciadv.abe7386
764 55. Huang C, Lokugamage KG, Rozovics JM, Narayanan K, Semler BL, Makino S.
765 SARS coronavirus nsp1 protein induces template-dependent endonucleolytic cleavage of
766 mRNAs: viral mRNAs are resistant to nsp1-induced RNA cleavage. PLoS Pathog. 2011;7:
767 e1002433. doi:10.1371/journal.ppat.1002433
768 56. Kamitani W, Huang C, Narayanan K, Lokugamage KG, Makino S. A two-pronged
769 strategy to suppress host protein synthesis by SARS coronavirus Nsp1 protein. Nat Struct Mol
770 Biol. 2009;16: 1134–1140. doi:10.1038/nsmb.1680
771 57. Kamitani W, Narayanan K, Huang C, Lokugamage K, Ikegami T, Ito N, et al. Severe
772 acute respiratory syndrome coronavirus nsp1 protein suppresses host gene expression by
773 promoting host mRNA degradation. PNAS. 2006;103: 12885–12890.
774 doi:10.1073/pnas.0603144103
775 58. Mendez AS, Ly M, González-Sánchez AM, Hartenian E, Ingolia NT, Cate JH, et al.
776 The N-terminal domain of SARS-CoV-2 nsp1 plays key roles in suppression of cellular gene
777 expression and preservation of viral gene expression. Cell Reports. 2021;37: 109841.
778 doi:10.1016/j.celrep.2021.109841
779 59. Sun G, Cui Q, Garcia G, Wang C, Zhang M, Arumugaswami V, et al. Comparative
780 transcriptomic analysis of SARS-CoV-2 infected cell model systems reveals differential
781 innate immune responses. Sci Rep. 2021;11: 17146. doi:10.1038/s41598-021-96462-w
782 60. Mu J, Fang Y, Yang Q, Shu T, Wang A, Huang M, et al. SARS-CoV-2 N protein
783 antagonizes type I interferon signaling by suppressing phosphorylation and nuclear
784 translocation of STAT1 and STAT2. Cell Discov. 2020;6: 1–4. doi:10.1038/s41421-020-
785 00208-3
786 61. Miorin L, Kehrer T, Sanchez-Aparicio MT, Zhang K, Cohen P, Patel RS, et al. SARS-
787 CoV-2 Orf6 hijacks Nup98 to block STAT nuclear import and antagonize interferon
788 signaling. Proc Natl Acad Sci U S A. 2020;117: 28344–28354. doi:10.1073/pnas.2016650117
789 62. Rebendenne A, Valadão ALC, Tauziet M, Maarifi G, Bonaventure B, McKellar J, et
790 al. SARS-CoV-2 triggers an MDA-5-dependent interferon response which is unable to control
791 replication in lung epithelial cells. J Virol. 2021; JVI.02415-20. doi:10.1128/JVI.02415-20
792 63. Banerjee A, El-Sayes N, Budylowski P, Jacob RA, Richard D, Maan H, et al.
793 Experimental and natural evidence of SARS-CoV-2-infection-induced activation of type I
794 interferon responses. iScience. 2021;24: 102477. doi:10.1016/j.isci.2021.102477
795 64. Yin X, Riva L, Pu Y, Martin-Sancho L, Kanamune J, Yamamoto Y, et al. MDA5
796 Governs the Innate Immune Response to SARS-CoV-2 in Lung Epithelial Cells. Cell Rep.
797 2021;34: 108628. doi:10.1016/j.celrep.2020.108628
798 65. Lei X, Dong X, Ma R, Wang W, Xiao X, Tian Z, et al. Activation and evasion of type
799 I interferon responses by SARS-CoV-2. Nat Commun. 2020;11: 3810. doi:10.1038/s41467-
800 020-17665-9
801 66. Stanifer ML, Kee C, Cortese M, Zumaran CM, Triana S, Mukenhirn M, et al. Critical
802 Role of Type III Interferon in Controlling SARS-CoV-2 Infection in Human Intestinal
803 Epithelial Cells. Cell Reports. 2020;32: 107863. doi:10.1016/j.celrep.2020.107863
804 67. Lamers MM, van der Vaart J, Knoops K, Riesebosch S, Breugem TI, Mykytyn AZ, et
805 al. An organoid-derived bronchioalveolar model for SARS-CoV-2 infection of human
806 alveolar type II-like cells. EMBO J. 2021;40: e105912. doi:10.15252/embj.2020105912
807 68. Stanifer ML, Kee C, Cortese M, Zumaran CM, Triana S, Mukenhirn M, et al. Critical
808 Role of Type III Interferon in Controlling SARS-CoV-2 Infection in Human Intestinal

809 Epithelial Cells. Cell Rep. 2020;32: 107863. doi:10.1016/j.celrep.2020.107863
810 69. Deng L, Zeng Q, Wang M, Cheng A, Jia R, Chen S, et al. Suppression of NF-κB
811 Activity: A Viral Immune Evasion Mechanism. Viruses. 2018;10: E409.
812 doi:10.3390/v10080409
813 70. Neufeldt CJ, Cerikan B, Cortese M, Frankish J, Lee J-Y, Plociennikowska A, et al.
814 SARS-CoV-2 infection induces a pro-inflammatory cytokine response through cGAS-STING
815 and NF-κB. 2020 Jul p. 2020.07.21.212639. doi:10.1101/2020.07.21.212639
816 71. Su C-M, Wang L, Yoo D. Activation of NF-κB and induction of proinflammatory
817 cytokine expressions mediated by ORF7a protein of SARS-CoV-2. Sci Rep. 2021;11: 13464.
818 doi:10.1038/s41598-021-92941-2
819 72. Li T, Kenney AD, Liu H, Fiches GN, Zhou D, Biswas A, et al. SARS-CoV-2 Nsp14
820 activates NF-κB signaling and induces IL-8 upregulation. bioRxiv. 2021; 2021.05.26.445787.
821 doi:10.1101/2021.05.26.445787
822 73. Li W, Qiao J, You Q, Zong S, Peng Q, Liu Y, et al. SARS-CoV-2 Nsp5 Activates NF-
823 κB Pathway by Upregulating SUMOylation of MAVS. Frontiers in Immunology. 2021;12:
824 4681. doi:10.3389/fimmu.2021.750969
825 74. Boreika R, Sitkauskiene B. Interleukin-32 in Pathogenesis of Atopic Diseases:
826 Proinflammatory or Anti-Inflammatory Role? Journal of Interferon & Cytokine Research.
827 2021;41: 235–243. doi:10.1089/jir.2020.0230
828 75. Li Y, Xie J, Xu X, Liu L, Wan Y, Liu Y, et al. Inducible Interleukin 32 (IL-32) Exerts
829 Extensive Antiviral Function via Selective Stimulation of Interferon λ1 (IFN-λ1) *. Journal of
830 Biological Chemistry. 2013;288: 20927–20941. doi:10.1074/jbc.M112.440115
831 76. Nold MF, Nold-Petry CA, Pott GB, Zepp JA, Saavedra MT, Kim S-H, et al.
832 Endogenous IL-32 controls cytokine and HIV-1 production. J Immunol. 2008;181: 557–565.
833 doi:10.4049/jimmunol.181.1.557
834 77. Li W, Sun W, Liu L, Yang F, Li Y, Chen Y, et al. IL-32: A Host Proinflammatory
835 Factor against Influenza Viral Replication Is Upregulated by Aberrant Epigenetic
836 Modifications during Influenza A Virus Infection. The Journal of Immunology. 2010;185:
837 5056–5065. doi:10.4049/jimmunol.0902667
838 78. Kim S-H, Han S-Y, Azam T, Yoon D-Y, Dinarello CA. Interleukin-32: a cytokine and
839 inducer of TNFalpha. Immunity. 2005;22: 131–142. doi:10.1016/j.immuni.2004.12.003
840 79. Khabar KSA, Al-Zoghaibi F, Al-Ahdal MN, Murayama T, Dhalla M, Mukaida N, et
841 al. The α Chemokine, Interleukin 8, Inhibits the Antiviral Action of Interferon α. J Exp Med.
842 1997;186: 1077–1085.
843 80. Pollicino T, Bellinghieri L, Restuccia A, Raffa G, Musolino C, Alibrandi A, et al.
844 Hepatitis B virus (HBV) induces the expression of interleukin-8 that in turn reduces HBV
845 sensitivity to interferon-alpha. Virology. 2013;444: 317–328. doi:10.1016/j.virol.2013.06.028
846 81. Kambara H, Niazi F, Kostadinova L, Moonka DK, Siegel CT, Post AB, et al. Negative
847 regulation of the interferon response by an interferon-induced long non-coding RNA. Nucleic
848 Acids Res. 2014;42: 10668–80. doi:10.1093/nar/gku713
849 82. Peng X, Gralinski L, Armour CD, Ferris MT, Thomas MJ, Proll S, et al. Unique
850 signatures of long noncoding RNA expression in response to virus infection and altered innate
851 immune signaling. MBio. 2010;1. doi:10.1128/mBio.00206-10
852 83. Ouyang J, Zhu X, Chen Y, Wei H, Chen Q, Chi X, et al. NRAV, a long noncoding
853 RNA, modulates antiviral responses through suppression of interferon-stimulated gene
854 transcription. Cell Host Microbe. 2014;16: 616–26. doi:10.1016/j.chom.2014.10.001
855 84. Du M, Yuan L, Tan X, Huang D, Wang X, Zheng Z, et al. The LPS-inducible lncRNA
856 Mirt2 is a negative regulator of inflammation. Nat Commun. 2017;8: 2049.
857 doi:10.1038/s41467-017-02229-1
858 85. Meydan C, Madrer N, Soreq H. The Neat Dance of COVID-19: NEAT1, DANCR,

859 and Co-Modulated Cholinergic RNAs Link to Inflammation. Frontiers in Immunology.
860 2020;11. Available: https://www.frontiersin.org/article/10.3389/fimmu.2020.590870
861 86. Saha C, Laha S, Chatterjee R, Bhattacharyya NP. Co-Regulation of Protein Coding
862 Genes by Transcription Factor and Long Non-Coding RNA in SARS-CoV-2 Infected Cells:
863 An In Silico Analysis. Noncoding RNA. 2021;7: 74. doi:10.3390/ncrna7040074
864 87. Vishnubalaji R, Shaath H, Alajez NM. Protein Coding and Long Noncoding RNA
865 (lncRNA) Transcriptional Landscape in SARS-CoV-2 Infected Bronchial Epithelial Cells
866 Highlight a Role for Interferon and Inflammatory Response. Genes (Basel). 2020;11: E760.
867 doi:10.3390/genes11070760
868 88. Mukherjee S, Banerjee B, Karasik D, Frenkel-Morgenstern M. mRNA-lncRNA Co-
869 Expression Network Analysis Reveals the Role of lncRNAs in Immune Dysfunction during
870 Severe SARS-CoV-2 Infection. Viruses. 2021;13: 402. doi:10.3390/v13030402
871 89. Combredet C, Labrousse V, Mollet L, Lorin C, Delebecque F, Hurtrel B, et al. A
872 Molecularly Cloned Schwarz Strain of Measles Virus Vaccine Induces Strong Immune
873 Responses in Macaques and Transgenic Mice. Journal of Virology. 2003;77: 11546–11554.
874 doi:10.1128/JVI.77.21.11546-11554.2003
875 90. Babraham Bioinformatics - Trim Galore! [cited 21 Feb 2022]. Available:
876 https://www.bioinformatics.babraham.ac.uk/projects/trim_galore/
877 91. Babraham Bioinformatics - FastQC A Quality Control tool for High Throughput
878 Sequence Data. [cited 21 Feb 2022]. Available:
879 https://www.bioinformatics.babraham.ac.uk/projects/fastqc/
880 92. Martin M. Cutadapt removes adapter sequences from high-throughput sequencing
881 reads. EMBnet.journal. 2011;17: 10–12. doi:http://dx.doi.org/10.14806/ej.17.1.200
882 93. Dobin A, Davis CA, Schlesinger F, Drenkow J, Zaleski C, Jha S, et al. STAR:
883 ultrafast universal RNA-seq aligner. Bioinformatics. 2013;29: 15–21.
884 doi:10.1093/bioinformatics/bts635
885 94. Li H, Handsaker B, Wysoker A, Fennell T, Ruan J, Homer N, et al. The Sequence
886 Alignment/Map format and SAMtools. Bioinformatics. 2009;25: 2078–9.
887 doi:10.1093/bioinformatics/btp352
888 95. Ramírez F, Ryan DP, Grüning B, Bhardwaj V, Kilpert F, Richter AS, et al.
889 deepTools2: a next generation web server for deep-sequencing data analysis. Nucleic Acids
890 Res. 2016;44: W160-165. doi:10.1093/nar/gkw257
891 96. Trapnell C, Williams BA, Pertea G, Mortazavi A, Kwan G, van Baren MJ, et al.
892 Transcript assembly and quantification by RNA-Seq reveals unannotated transcripts and
893 isoform switching during cell differentiation. Nat Biotechnol. 2010;28: 511–515.
894 doi:10.1038/nbt.1621
895 97. Quinlan AR, Hall IM. BEDTools: a flexible suite of utilities for comparing genomic
896 features. Bioinformatics. 2010;26: 841–2. doi:10.1093/bioinformatics/btq033
897 98. Liao Y, Smyth GK, Shi W. featureCounts: an efficient general purpose program for
898 assigning sequence reads to genomic features. Bioinformatics. 2014;30: 923–930.
899 doi:10.1093/bioinformatics/btt656
900 99. R Core Team. R: A Language and Environment for Statistical Computing. Vienna,
901 Austria; 2017.
902 100. Love MI, Huber W, Anders S. Moderated estimation of fold change and dispersion for
903 RNA-seq data with DESeq2. Genome Biol. 2014;15: 550. doi:10.1186/s13059-014-0550-8
904 101. Huang DW, Sherman BT, Lempicki RA. Systematic and integrative analysis of large
905 gene lists using DAVID bioinformatics resources. Nat Protoc. 2009;4: 44–57.
906 doi:10.1038/nprot.2008.211
907 102. Huang DW, Sherman BT, Lempicki RA. Bioinformatics enrichment tools: paths
908 toward the comprehensive functional analysis of large gene lists. Nucleic Acids Res. 2009;37:

1–13. doi:10.1093/nar/gkn923
103. Zhang Y, Liu T, Meyer CA, Eeckhoute J, Johnson DS, Bernstein BE, et al. Model-based Analysis of ChIP-Seq (MACS). Genome Biology. 2008;9: R137. doi:10.1186/gb-2008-9-9-r137
104. EMBOSS: fuzznuc. [cited 21 Feb 2022]. Available: http://emboss.toulouse.inra.fr/cgi-bin/emboss/fuzznuc
105. Chen FE, Huang DB, Chen YQ, Ghosh G. Crystal structure of p50/p65 heterodimer of transcription factor NF-kappaB bound to DNA. Nature. 1998;391: 410–413. doi:10.1038/34956

920 **Additional information.**

921

922 Table S1. Differential expression analysis of mRNAs (infected S^+ vs mock, infected S^+ vs bystander,
923 and bystander vs mock).

924

925 Table S2. Differential expression analysis of lncRNAs (infected S^+ vs mock, infected S^+ vs bystander,
926 and bystander vs mock).

927

928 Table S3. Differential expression analysis of unannotated RNAs (infected S^+ vs mock, infected S^+ vs
929 bystander, and bystander vs mock).

930

931 Table S4. Gene overlap between DE-seq from our 'sorted vs mock' samples and 'mixed vs mock'
932 data re-analyzed from Blanco-Melo *et al.* 2020 (MOI of 0.2).

933

934 Table S5. This table shows known NF-κB target mRNAs, as well as predicted NF-κB target lncRNAs
935 and unreferenced RNAs, among upregulated RNAs in S^+ vs mock cells.

936

937 Table S6. RT-qPCR primer sequences

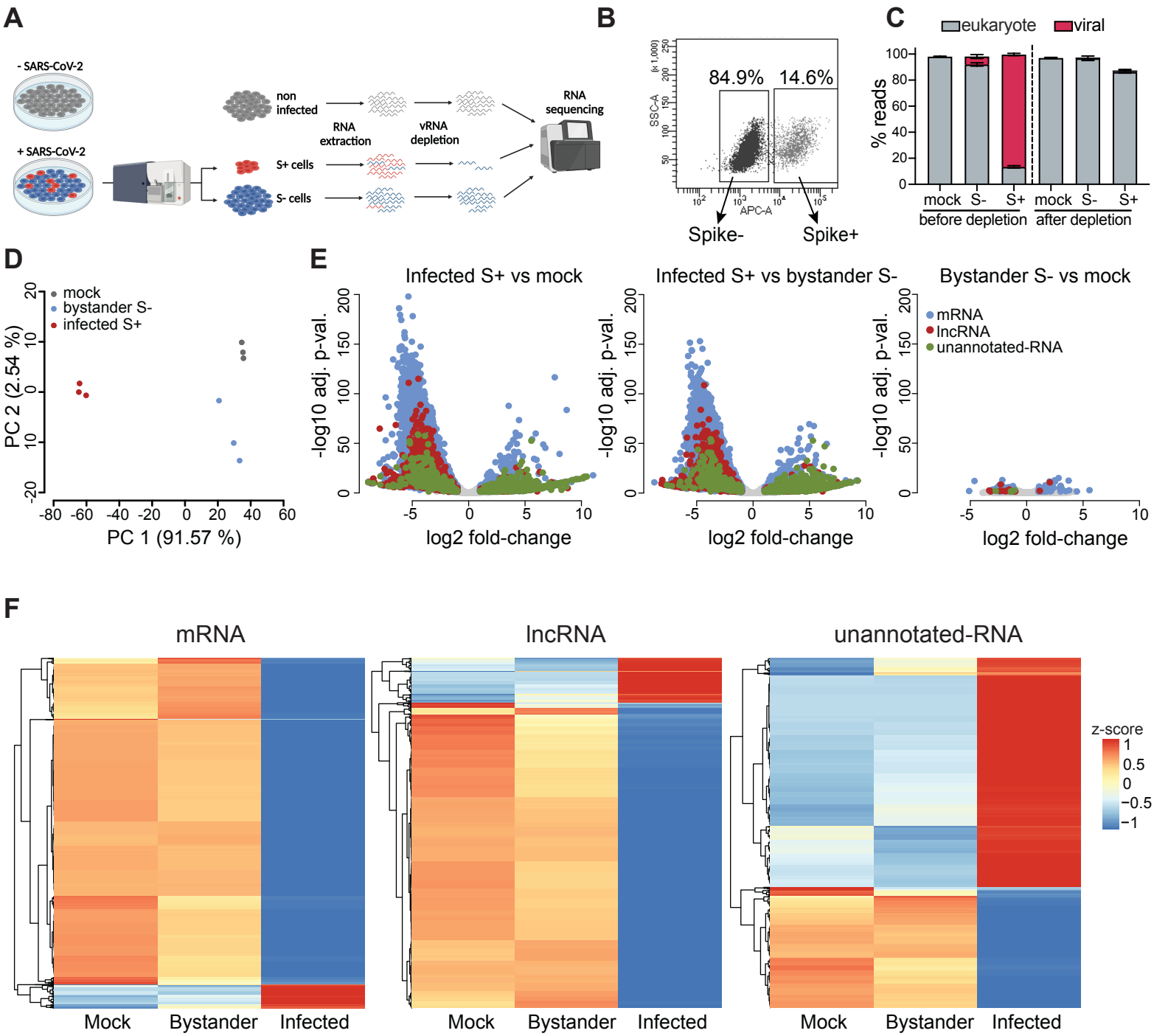

Figure 1. Differential transcriptomic analysis of SARS-CoV-2 infected and bystander lung cells. (**A**) Scheme summarizing the experimental workflow. A549-ACE2 cells were infected with SARS-CoV-2 at a MOI of 1 for 24h, stained for viral S protein followed by flow cytometry sorting of productively infected (S+) and bystander (S-) cells. Total RNA from mock, S- and S+ cells was depleted of ribosomal and viral RNAs and sequenced. (**B**) Representative FACS plot of S protein staining used for sorting productively infected cells. (**C**) Percentage of reads in libraries originating from human genome or SARS-CoV-2 sequence, before and after depletion of viral reads. (**D**) PCA plot based on the top 500 most variable genes between mock, bystander (S-) and infected (S+) cells. (**E**) Volcano plots presenting distribution of classes of transcripts (mRNA-blue, lncRNA-red, unannotated-green) based on their log2 fold-change for 3 comparisons: infected cells vs mock, infected cells vs bystander and bystander vs mock. (**F**) Heatmaps presenting z-score of log2 normalized counts for all differentially expressed genes between mock, bystander and infected cells, separated for mRNAs, lncRNAs and unannotated RNA.

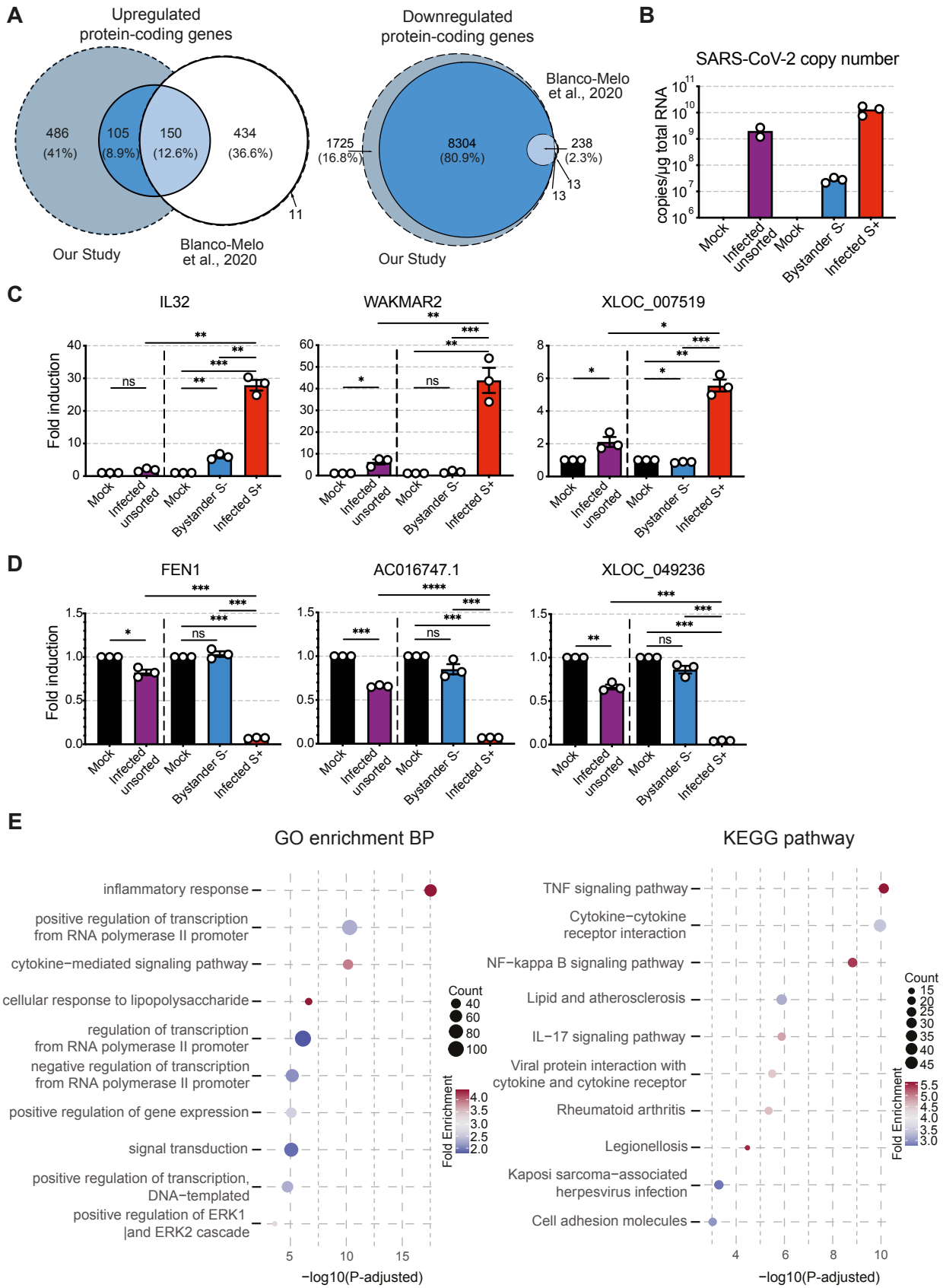

Figure 2. Separating lung cells based on the expression of the viral S protein improved discovery of DEGs. (**A**) Venn diagram representing gene overlap between DE-seq from sorted vs mock samples and mixed vs mock data re-analyzed from Blanco-Melo et al. 2020 (MOI of 0.2). The genes were defined as upregulated if log2 fold change was equal or above 1 (right panel) and equal or below -1 for downregulated genes (left panel). Genes were defined as expressed when they were represented by at least 10 normalized reads in each replicate. The solid lines and central overlap show the genes that appear in both datasets while dashed gray zones outline genes detected in only one of the two datasets. (**B**) RT-qPCR quantification of viral genome copy number per µg of total RNA extracted from A549-ACE2 cells infected by SARS-CoV-2 at a MOI of 1, analyzed either in bulk (left side of graph, n=2 independent experiments, line at mean) or post-sorting based on Spike protein expression, allowing distinction between productively infected and bystander subpopulations (right side of graph, n=3 experiments, line at mean). (**C-D**) RT-qPCR quantification of mRNA, lncRNA, and unannotated-RNA, that were identified as upregulated (**C**) or downregulated (**D**) upon infection by SARS-CoV-2 in the RNA-seq analysis, in total RNA extracted from A549-ACE2 cells infected with SARS-CoV-2 at a MOI of 1, analyzed either in bulk (left side of graph) or post-sorting based on Spike protein expression (right side of graph, normalized fold change over mock-infected, n=3 independent experiments, ratio-paired t test, line at mean ± SEM). (**E**) Top 10 enriched GO terms for Biological Process (BP) and KEGG pathways from DAVID database ranked by the adjusted p-value (Benjamini), for upregulated mRNAs identified in RNA-Seq comparison between infected vs mock cells.

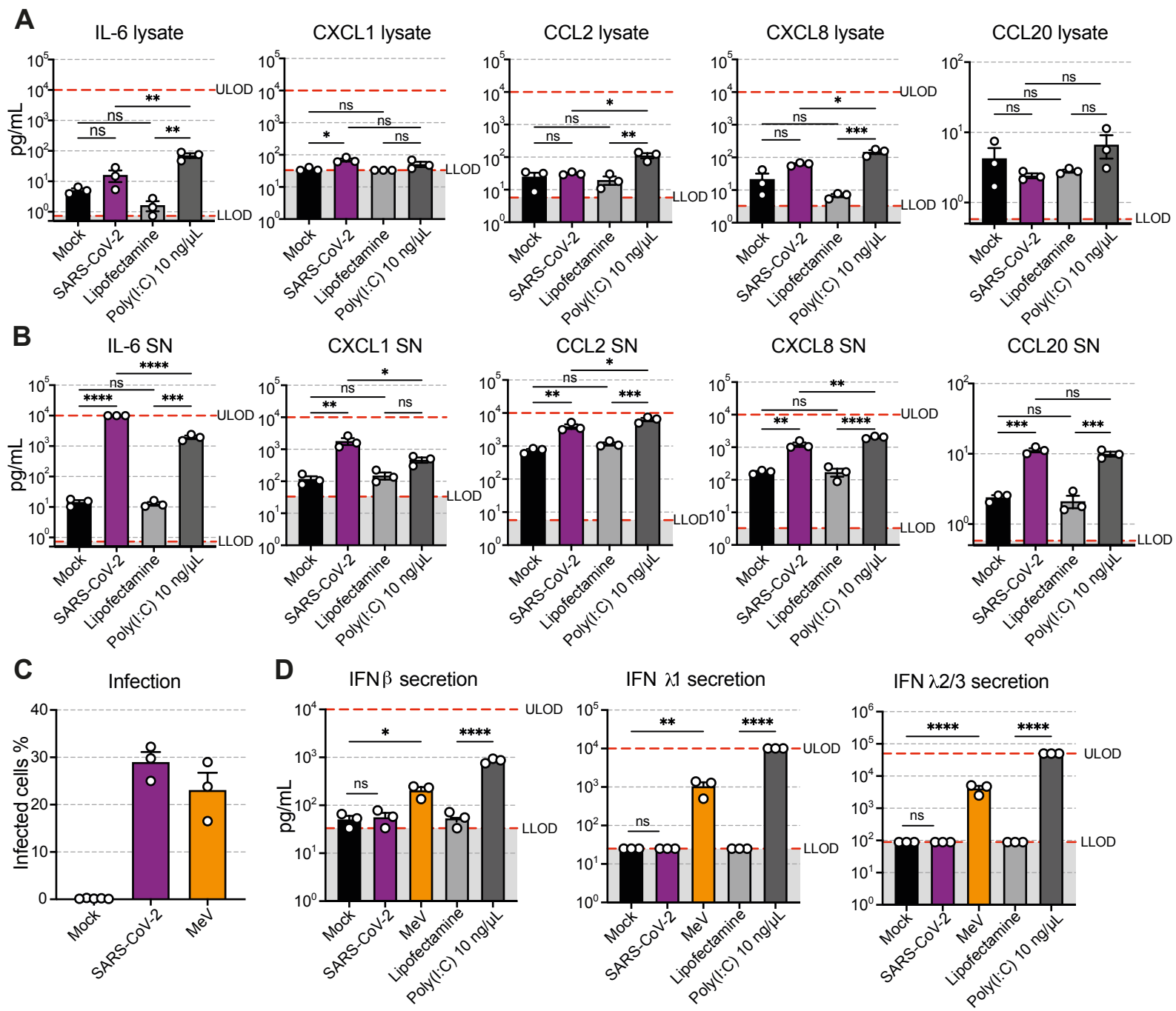

Figure 3. Inflammatory cytokines, but not IFNs, are produced and secreted by infected cells. (**A**) Quantification of the indicated chemokines by cytometry bead array in A549-ACE2 cell lysates obtained 24 hours post mock-infection or infected with SARS-CoV-2 at a MOI of 1, or post-treatment with transfectant alone or in combination with 10 ng/µL of Poly(I:C) (n=3 independent experiments, paired One-Way ANOVA with Turkey's post-test, line at mean ± SEM). (**B**) Quantification of the indicated chemokines by cytometry bead array in supernatant (SN) of cells shown in (A) (n=3 independent experiments, paired One-Way ANOVA with Turkey's post-test, line at mean ± SEM). (**C**) Percentages of infected A549-ACE2 cells 24 hours post infection (MOI of 1) with SARS-CoV-2 or Measles virus expressing GFP (MeV), quantified by flow cytometry using Spike protein staining and GFP expression, respectively (n=3 independent experiments, line at mean ± SEM). (**D**) Quantification of secretion of IFNβ, IFNλ1 and IFNλ2/3 by cytometry bead arrays in supernatant of A549-ACE2 cells 24 hours post-infection with SARS-CoV-2 or MeV (MOI of 1), or post-treatment with transfectant alone or in combination with 10 ng/µL of Poly(I:C) (n=3 independent experiments, One-Way ANOVA with Šídák's post-test, line at mean ± SEM).
ULOD: Upper Limit of Detection; LLOD: Lower Limit of Detection

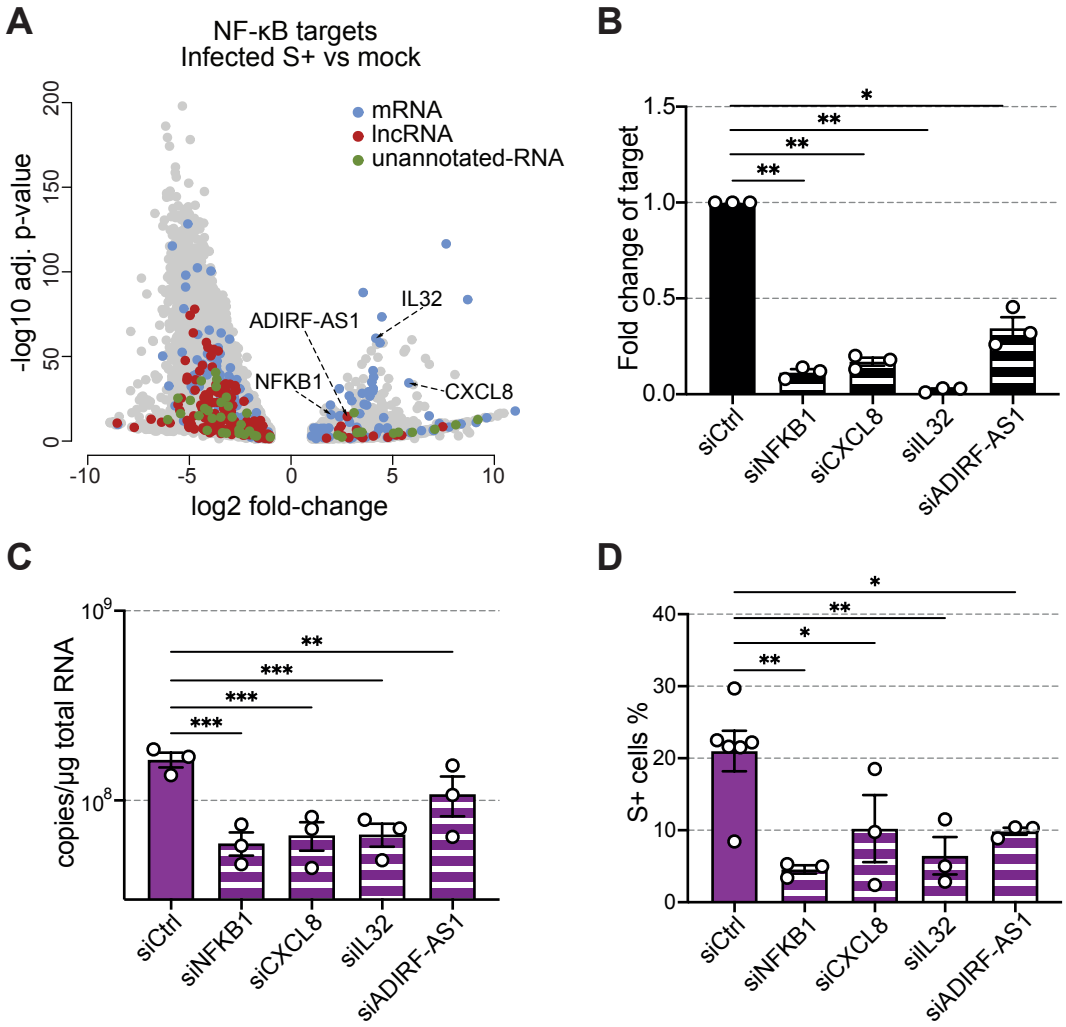

Figure 4. Upregulated NF-κB target genes contribute to an optimal SARS-CoV-2 replication. (**A**) Volcano plot presenting log2 fold change of RNA expression from RNA-seq analysis between S+ and mock cells and showing known NF-κB target mRNAs (labeled in blue), as well as NF-κB target lncRNAs (red) and unannotated RNAs (green) predicted from ChIP and motif analysis. (**B**) RT-qPCR quantification of knock-down efficiency of indicated transcripts in A549-ACE2 cells, 48 hours post-transfection with a pool of siRNAs targeting indicated genes (normalized fold change over control siRNA, n=3 independent experiments, ratio-paired t test, line at mean ± SEM). (**C**) RT-qPCR quantification of viral genome copy number per µg of total RNA extracted from A549-ACE2 cells, with indicated genes knocked down, 24 hours after infection with SARS-CoV-2 (MOI of 1) (n=3 independent experiments, One-Way ANOVA with Dunnett's post-test, line at mean ± SEM). (**D**) Percentages of infected A549-ACE2 cells, with selected genes knocked-down, 24 hours post infection with SARS-CoV-2 (MOI of 1), quantified by flow cytometry using Spike protein staining (n=3 independent experiments, mixed model one-Way ANOVA with Dunnett's post-test, line at mean ± SEM).

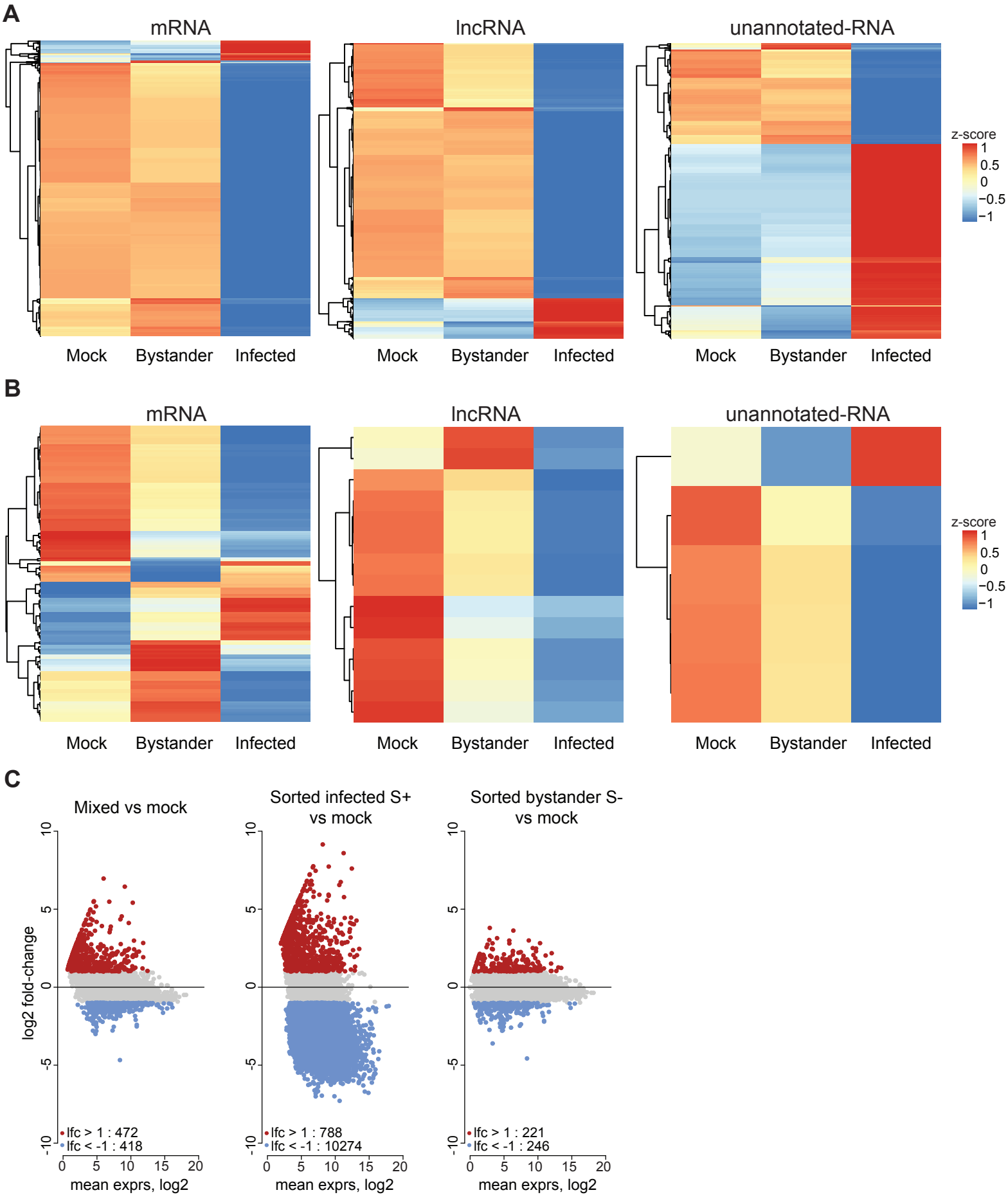

Figure S1. (**A-B**) Heatmaps presenting z-score of log2 normalized counts for differentially expressed genes between (**A**) S+ vs S- cells or (**B**) S- vs mock-infected treated cells, separated for mRNAs, lncRNAs and unannotated RNAs. (**C**) MA plot showing the response to infection of an artificially reconstructed mixed cell population (80% bystander, 20% infected, left) compared to cells sorted based on the expression of the viral protein Spike (infected, middle; bystander, right).

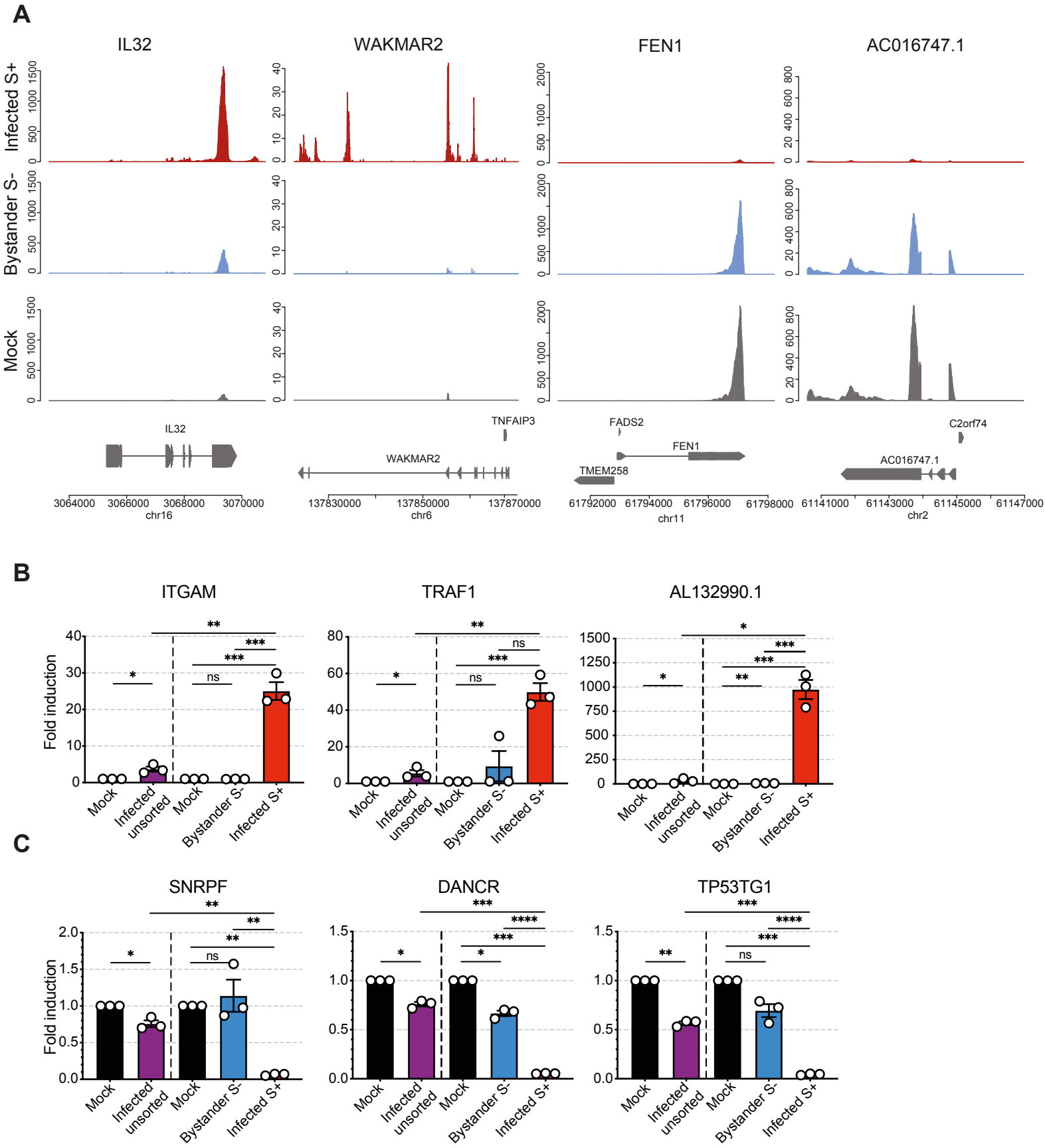

Figure S2. (**A**) Visualization of read coverage (tag/nucleotide) from polyA+ RNA-seq normalized on ERCC reads for IL32, WAKMAR2, FEN1 and AC016747.1. (**B-C**) RT-qPCR quantification of mRNAs and lncRNAs that are either upregulated (**B**) or downregulated (**C**) upon infection with SARS-CoV-2, in total RNA extracted from A549-ACE2 cells infected at an MOI of 1, analyzed either in bulk (left side of graph) or post sorting based on Spike protein (right side of graph, normalized fold change over mock-infected, n=3 independent experiments, ratio-paired t test, line at mean ± SEM).

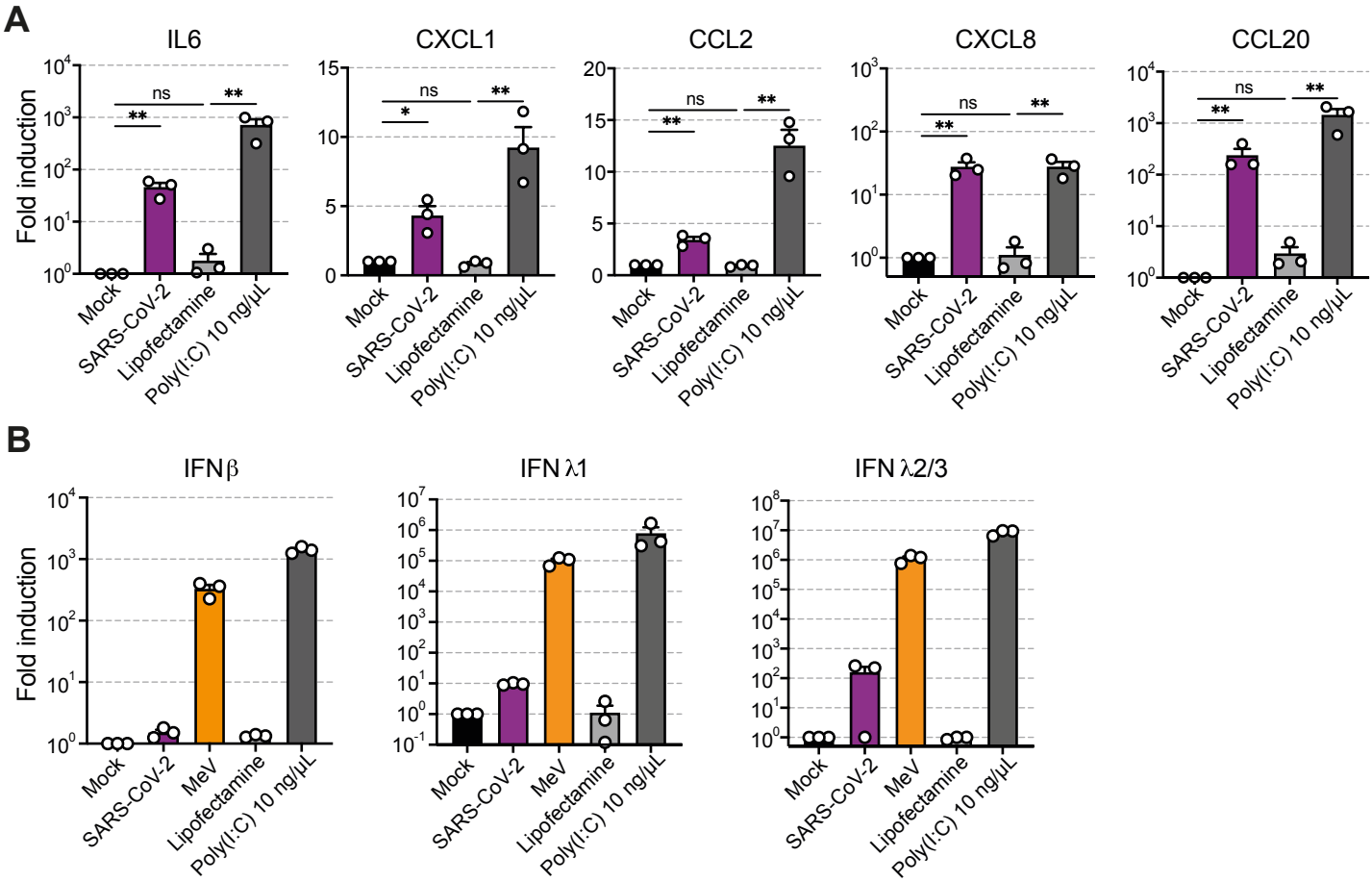

Figure S3. (**A**) RT-qPCR quantification of transcript induction of indicated chemokines in A549-ACE2 cells, 24 hours post infection with SARS-CoV-2 (MOI of 1) or post-treatment with transfectant alone or in combination with 10 ng/µL of Poly(I:C) (normalized fold change over mock-infected, n=3 independent experiments, ratio-paired t test, line at mean ± SEM). (**B**) RT-qPCR quantification of IFNβ, IFNλ1 and IFNλ2/3 transcripts induction in A549-ACE2 cells, 24 hours post infection at an MOI of 1 with SARS-CoV-2 or Measles virus expressing GFP (MeV) or post treatment with transfectant alone or in combination with 10 ng/µL of Poly(I:C) (normalized fold change over mock-infected, n=3 independent experiments, line at mean ± SEM).

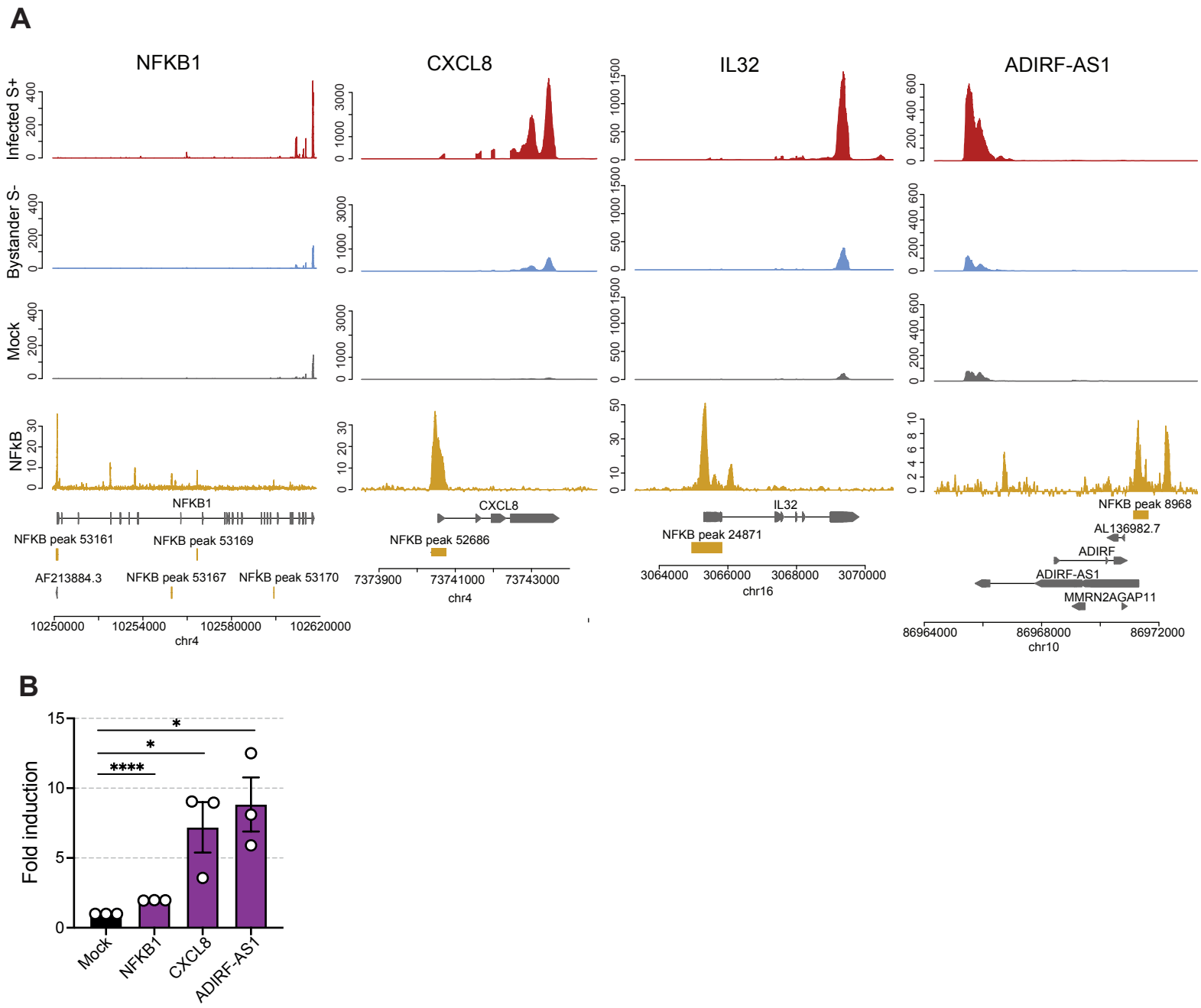

Figure S4. (**A**) Visualization of read coverage (tag/nucleotide) from polyA+ RNA-seq and ChIP-seq (IP – Input) at NFKB1, CXCL8, IL32 and ADIRF-AS1 loci. RNA-seq and ChIP-seq data were normalized independently, on ERCC reads for RNA-seq and on library size for ChIP-seq. (**B**) RT-qPCR quantification of NFKB1, CXCL8 and ADIRF-AS1 transcripts induction in A549-ACE2 cells, 24 hours post infection with SARS-CoV-2 (MOI of 1) (normalized fold change over mock-infected, n=3 independent experiments, ratio-paired t test, line at mean ± SEM).